Agricultural and Forest Meteorology 296 (2021) 108216

Contents lists available at ScienceDirect

Agricultural and Forest Meteorology

journal homepage: www.elsevier.com/locate/agrformet

Biases in open-path carbon dioxide flux measurements: Roles of instrument surface heat exchange and analyzer temperature sensitivity

M Julian Deventer [a,b,*], Tyler Roman [c], Ivan Bogoev [d], Randall K. Kolka [c], Matt Erickson [a], Xuhui Lee [e], John M. Baker [a,f], Dylan B. Millet [a], Timothy J. Griffis [a]

[a] University of Minnesota – Dept. Soil, Water & Climate, St. Paul, MN, USA
[b] ANECO Institut für Umweltschutz GmbH & Co, Hamburg, Germany
[c] US Forest Service – Northern Research Station Grand Rapids, Grand Rapids, MN, USA
[d] Campbell Scientific, Logan, UT, USA
[e] School of Forestry & Environmental Studies, Yale, New Haven, CT, USA
[f] US Department of Agriculture (ARS) – Soil and Water Management Research, St. Paul, MN, USA

A B S T R A C T

Eddy covariance (EC) measurements of ecosystem-atmosphere carbon dioxide (CO_2) exchange provide the most direct assessment of the terrestrial carbon cycle. Measurement biases for open-path (OP) CO_2 concentration and flux measurements have been reported for over 30 years, but their origin and appropriate correction approach remain unresolved. Here, we quantify the impacts of OP biases on carbon and radiative forcing budgets for a sub-boreal wetland. Comparison with a reference closed-path (CP) system indicates that a systematic OP flux bias (0.54 μmol m^{-2} s^{-1}) persists for all seasons leading to a 110% overestimate of the ecosystem CO_2 sink (cumulative error of 78 gC m^{-2}). Two potential OP bias sources are considered: Sensor-path heat exchange (SPHE) and analyzer temperature sensitivity. We examined potential OP correction approaches including: i) Fast temperature measurements within the measurement path and sensor surfaces; ii) Previously published parameterizations; and iii) Optimization algorithms. The measurements revealed year-round average temperature and heat flux gradients of 2.9 °C and 16 W m^{-2} between the bottom sensor surfaces and atmosphere, indicating SPHE-induced OP bias. However, measured SPHE correlated poorly with the observed differences between OP and CP CO_2 fluxes. While previously proposed nominally universal corrections for SPHE reduced the cumulative OP bias, they led to either systematic under-correction (by 38.1 gC m^{-2}) or to systematic over-correction (by 17-37 gC m^{-2}). The resulting budget errors exceeded CP random uncertainty and change the sign of the overall carbon and radiative forcing budgets. Analysis of OP calibration residuals as a function of temperature revealed a sensitivity of 5 μmol m^{-3} K^{-1}. This temperature sensitivity causes CO_2 calibration errors proportional to sample air fluctuations that can offset the observed growing season flux bias by 50%. Consequently, we call for a new OP correction framework that characterizes SPHE- and temperature-induced CO_2 measurement errors.

1. Introduction

Networks of continuous trace gas flux measurements provide the most direct tool for quantifying global biogeochemical cycles of greenhouse gases (GHGs), and are critical for monitoring ecosystem responses to climate variations. The current generation of fast-response gas analyzers is able to directly resolve temporal and spatial variations in net ecosystem exchange (NEE) of the 4 most abundant greenhouse gases (GHGs)—water vapor (H_2O), carbon dioxide (CO_2), methane (CH_4), and nitrous oxide (N_2O)—by eddy covariance (EC) (Nemitz et al., 2018; Rebmann et al., 2018). Globally synthesized long-term measurements of these GHG fluxes help constrain terrestrial carbon and nitrogen cycling and the radiative forcing contributions of different ecosystems across the globe. Such measurements are key to understanding the variability and trajectory of the climate system (e.g. Petrescu et al., 2015; Baldocchi et al., 2016).

Necessary for this endeavor are fast-response and accurate instruments that can resolve atmospheric scalar fluctuations near their background levels across a wide range of hydro-meteorological conditions. Accurate measurements of CO_2 fluxes are of particular interest given their importance for climate change and because they form the foundation for understanding the carbon balance of ecosystems. EC-based CO_2 flux measurements date back to the early 1970s (e.g. Desjardins, 1974), but did not gain global popularity until the commercial development of fast response sonic anemometers and low-power open-path (OP) infrared gas analyzers (e.g. Jones et al., 1967; Bingham et al., 1978; Heikinheimo et al., 1989).

Despite over four intervening decades of measurements, technological and methodological refinements, debates about measurement artifacts for OP gas analyzers persist. In particular, there are now many

* Corresponding author.
E-mail address: deventer@umn.edu (M.J. Deventer).

https://doi.org/10.1016/j.agrformet.2020.108216
Received 9 April 2020; Received in revised form 4 August 2020; Accepted 11 October 2020

reports of physiologically unreasonable OP-derived net CO_2 uptake fluxes during photosynthetically inactive periods and in ecosystems lacking photosynthetically active vegetation (e.g. Hirata et al., 2005; Amiro, 2010; Welp et al., 2007; Wohlfahrt et al., 2008; Ono et al., 2008; Lafleur and Humphreys, 2008; Ma et al., 2014; Wang et al., 2016; Helbig et al., 2016). Other studies have reported systematic discrepancies between OP and concurrent closed-path (CP) EC or chamber measurements that persist into the growing season, manifesting as smaller-magnitude positive and larger-magnitude negative OP-derived fluxes (e.g. Anthoni et al., 2002; Ono et al., 2008; Järvi et al., 2009; Kittler et al., 2017; Holl et al., 2019). In a meta-study, Wang et al. (2017) found evidence of cold-season NEE open-path sensor artifacts across the majority of examined FLUXNET sites. Similar findings have been reported in the marine flux community: for example, Butterworth and Else (2018) report that net CO_2 uptake fluxes measured via OP EC over land-fast sea ice were on average 25 times larger than chamber-derived fluxes. Such discrepancies have now been reported for over 30 years (e.g., Broecker et al., 1986).

The above findings have spurred an ongoing and unresolved debate on the underlying mechanisms driving OP biases. Discussions evolved around the Webb-Pearman-Leuning (WPL) formulations that account for heat-, water vapor-, and static pressure-driven air density fluctuations, which are required for OP flux calculations (Webb et al., 1980; Lee and Massman 2011). Massman and Lee (2002) argued that in complex terrain (e.g. for tall canopies) and under high wind speeds, the WPL pressure variance term becomes significant, contradicting the common practice of neglecting this effect. Under such conditions, erroneous sonic temperature and consequently sensible heat flux measurements were proposed to bias the OP flux calculations (Grelle and Lindroth, 1996). Subsequently, implausible OP fluxes were identified over simple terrain, and under low wind speeds; such conditions render the above pressure-related mechanisms unlikely (Ono et al., 2008). Others have postulated that thermal expansion and contraction of the instrument's frame, contamination/degradation of optical components, instrument calibration drift, or incomplete surface energy balance closure could explain the observed OP flux artifacts (Serrano-Ortiz et al., 2008; Fratini et al., 2014; Liu et al., 2006).

Two proposed bias mechanisms have gained the most persistent attention in the EC community, specifically artifacts related to: 1) spectroscopic corrections; and 2) sensor path heat exchange (SPHE). Edson et al. (2011), Kondo et al. (2014), Bogoev et al. (2015), Helbig et al. (2016), Wang et al. (2016), and Russel et al. (2019) showed that inaccurate/insufficient spectroscopic corrections (accounting for absorption line broadening due to barometric pressure, air temperature and dilution gases e.g. H_2O) led to biased fluxes with two widely-used commercial non-dispersive infrared (NDIR) OP gas analyzers (EC150, Campbell Scientific Inc., Logan, Utah, USA; LI-7500, LI-COR Biosciences, Lincoln, Nebraska, USA). In contrast, Burba et al. (2019) argue that aside from water vapor broadening, no spectroscopic corrections are needed for the LI-7500 since the Boltzman distributions are well-sampled, and thus temperature sensitivities are essentially eliminated. Steered by frequent reports of implausible LI-7500 flux measurements under cold conditions, Grelle and Burba (2007) found evidence that heat exchange from OP sensor surfaces and from air within the measurement path is the dominant cause of OP measurement bias. An influential review on this mechanism (Burba et al., 2008) has informed the implementation of SPHE corrections in the widely-used "EddyPro" (LI-COR, Biosciences) open-source EC processing software. Since then, efforts have been initiated to revise previously-published NEE budgets across regional flux networks to account for sensor surface heating biases (e.g. Reverter et al. 2011).

Despite this broad implementation, only a few studies have experimentally tested whether SPHE is the main driver of OP-derived flux biases at their sites, and if the proposed corrections yield satisfactory constraints (Wohlfahrt et al., 2008; Järvi et al., 2009; Haslwanter et al., 2009; Kittler et al., 2017). This lack of systematic assessment is problematic given the extensive use of OP-derived flux data within the community. Based on a review of site documentation for the BASE data products (AMERIFLUX 2019), early-generation LI-7500 instruments have been deployed at more than 50 flux towers across the U.S. and Canada, yielding >300 site-years and >30,000 unique downloads of potentially biased flux data. This is a conservative estimate, as instrumentation documentation is not provided publicly for a large number of sites. Furthermore, Wang et al. (2017) report similar biases for later-generation OP sensors that consume lower power and are intended to be bias-free.

Here we re-evaluate the currently-proposed corrections for SPHE-induced flux biases at a cold sub-boreal wetland site *via* concurrent OP and CP CO_2 flux measurements. Specifically, we examine the uncertainties and the systematic biases among the different correction methods outlined above, and the implications for assessing ecosystem carbon balance and radiative forcing based on eddy flux measurements of CO_2 and CH_4.

2. Methods

2.1. Measurement site and instrumentation

Eddy covariance measurements were carried out at the Bog Lake Peatland flux tower (US-MBP on AMERIFLUX) in the USDA Forest Service's Marcell Experimental Forest (47.505 N, 93.489 W, Minnesota, USA). The tower lies in an open natural peatland with short vegetation dominated by peat mosses (*Sphagnum ssp*). The climate is cold continental with warm summers, characterized by mean annual precipitation and temperature (1961-2009 reference period) of 780 mm and 3.4°C, respectively. The snow-covered period usually starts in November and typically lasts for ~120 days. The site's ecology, hydrology, and EC-derived carbon balances have been described previously in Shurpali et al. (1993, 1995), Sebestyen et al. (2011), Olson et al. (2013), and Deventer et al. (2019).

Three-dimensional wind velocity and sonic temperature measurements were made using an ultrasonic anemometer (CSAT-3, Campbell Scientific Inc., Logan, Utah, USA) mounted 2.4 m above-canopy. An OP CO_2 and H_2O infrared gas analyzer (LI-7500 from 04/2009-07/2015, LI-7500A from 08/2015-present; LI-COR Biosciences Inc., Lincoln, Nebraska, USA) was positioned at the same height as the sonic anemometer (in reference to the center of its measurement path) and offset by 10 cm to the east. For a short period (2/15/2019 to 3/19/2019) the LI-7500A was replaced by an identical sensor type of more recent serial number. During this time the original LI7500A was refurbished and factory-calibrated by LI-COR. The OP sensor was tilted by ~40 degrees relative to the sonic anemometer to reduce retention of water droplets and particles on optical surfaces. The LI-7500A chopper housing was maintained at 20°C year-round, matching the hard-coded factory setup for the earlier-generation LI-7500. In this way the analyzer's heat emissions remained constant between both versions. Note that with the introduction of the LI-7500A/RS updates, an optional "winter setting" became available for this analyzer. In winter mode the power consumption and heat production from the chopper motor housing are reduced to mitigate sensor-path heat exchange. This study did not evaluate the potential of the winter settings to minimize wintertime OP biases.

Starting in November 2018, CO_2 and H_2O (dry) mole fractions were also measured with a CP analyzer (LI-7200, LI-COR Biosciences Inc.). Here, air was sampled through a 1 m insulated intake tube installed at the same height and offset 4 cm east from the sonic reference. The volumetric flow rate was maintained at ~14 l min^{-1}. Additionally, high-frequency CH_4 concentrations were measured with a low-power OP analyzer (LI-7700, LI-COR Biosciences Inc.) that was vertically aligned but offset 40 cm south from the sonic reference. Methane-specific flux calculations and uncertainties were described earlier by Deventer et al. (2019).

To monitor OP analyzer temperatures and calculate heat fluxes in the OP measurement path, fast ambient and sensor surface temperature measurements were made using fine-wire (FW) thermocouples (0.017 mm diameter; TT-T-40-SLE, OMEGA Engineering, Norwalk, CT, USA). These thermocouples were mounted in close proximity (≈1 cm) to the LI-7500(A) bottom and top windows, and either directly fixed to the white instrument surfaces or at ~3 cm vertical distance from those surfaces. To compare our FW measurements to the ones from Burba et al., (2008) we average the two point-measurements to obtain an estimate of LI-7500 optical path heat fluxes. Our method is different from the one deployed in Burba et al., (2008) who used platinum wire strung across the entire measurement volume. Comprehensive auxiliary measurements are routinely performed at Bog Lake Peatland, with descriptions provided by Sebestyen et al. (2011) and Deventer et al. (2019).

2.2. Traditional (WPL) open-path calculation: the default OP flux

We apply WPL theory to account for air density fluctuations in calculating OP-derived fluxes. For simplicity, we discuss only the carbon flux corrections here and formulate WPL in terms of the fluxes of water vapor and sensible heat. The resulting WPL-calculated flux (F_{OP}; kg m^{-2} s^{-1}) is hereafter designated the "default OP flux" (Webb et al., 1980):

$$F_{OP} = \overline{w'\rho_c'} + \mu\frac{\overline{\rho_c}}{\overline{\rho}_{dry}}E_0 + \frac{\overline{\rho_c}}{\overline{\rho}c_p\overline{T_a}}\left(1+\mu\frac{\overline{\rho_v}}{\overline{\rho}_{dry}}\right)H; \quad \mu = 1.6077, \tag{1}$$

where w is the vertical wind speed, ρ_c, ρ_v, ρ_{dry}, and ρ are the densities of CO_2, H_2O, dry air, and air (kg m^{-3}), E_0 is the H_2O flux (kg m^{-2} s^{-1}), c_p is the specific heat of air (J kg^{-1} K^{-1}), T_a is the air temperature (K), μ is the air:water molecular mass ratio (unitless), and H is the ecosystem sensible heat flux (W m^{-2}). Overbars denote time averages and primes denote turbulent fluctuations.

2.3. Open-path corrections accounting for sensor-path heat exchange (SPHE)

Several correction approaches for SPHE have been proposed. In the following we present the theoretical framework for each approach that will later be evaluated against reference fluxes from the CP system.

2.3.1. Parameterizing instrument heat fluxes based on controlled experiments: the "Burba" correction (BC)

Grelle and Burba (2007) found experimental evidence for SPHE that was greater than the actual ecosystem sensible heat fluxes (H), and that originated from sensor surfaces that were either a few degrees warmer or cooler than ambient air. Three hypotheses were proposed to explain this: (i) under cold conditions, electronic components can heat instrument surfaces to above-ambient temperatures (sensor self-heating); (ii) on clear days, solar radiation can heat exposed instrument surfaces to above-ambient temperatures (external heating); and (iii) on clear nights, radiative cooling can lead to below-ambient surface temperatures. Once air density fluctuations due to internal and external SPHE had been accounted for, Grelle and Burba (2007) and Burba et al. (2008) both reported good agreement between OP- and CP-derived CO_2 fluxes.

Burba et al. (2008) introduced three different methods (hereafter designated as Burba Corrections, "BC") to account for the above effects; these are distinct from the traditional WPL terms. The BC methods are specific to the LI-7500 model and rely either on fast temperature measurements within the measurement path or are based on empirical models derived from controlled experiments. The first method is informed by direct heat flux measurements within the optical path of the gas analyzer, and is thus recommended by Burba et al. (2008). The latter two methods have the advantage that they can be applied (as universal) to historic datasets, though without any direct validation. Owing to the extra investment in measurements and data processing for direct SPHE measurements, to date there have been no independent studies evaluating their potential for OP corrections. However, a few studies have evaluated the two nominally universal BC corrections (e.g. Järvi et al., 2009; Helbig et al. 2016; Kittler et al., 2017).

Within the BC framework, the sensible heat flux H in Eq. 1 is replaced by the measurement path sensible heat flux S (W m^{-2}), thereby taking into account additional heat exchange from the instrument surfaces (S_{OP}). If temperatures within the optical-path are measured, SPHE is calculated following:

$$S = \rho c_p \overline{w' T_{OP}'}, \tag{2}$$

where T_{OP} is the temperature measured within the LI-7500 optical-path. If S is not measured directly, the BC method provides a parameterization:

$$S = H + S_{OP}, \text{with } S_{OP} = S_{bot} + S_{top} + 0.15\, S_{spar}. \tag{3}$$

Here, S_{OP} (W m^{-2}) is the instrument surface heat flux estimated from the sum of heat fluxes from the bottom, top, and spars of the instrument (Grelle & Burba 2007; Burba et al., 2008). In controlled experiments, the authors observed a linear relationship between instrument surface temperatures (T_s) and ambient meteorological conditions, which was then formulated either as a simple linear regression of T_s vs. T_a (referred to here as the BC SLR approach) or as a multiple linear regression that also includes radiation components and wind speed as independent variables (BC MLR approach):

$$T_{S,SLR} = d_1\, T_a + d_0, \tag{4}$$

or

$$T_{S,MLR} = d_1\, T_a + d_2\, K + d_3\, U + d_0 + T_a, \tag{5}$$

where U is horizontal wind speed (m s^{-1}), and K is radiation flux (W m^{-2}), specifically incoming shortwave during day- and incoming longwave radiation during nighttime. The SLR and MLR fitting coefficients (d) are provided by Burba et al. (2008), and are differentiated by day- vs. night-time conditions. Surface temperatures are then passed to model equations following Nobel (1983) that estimate instrument surface heat flux components based on the surface-to-ambient temperature gradient scaled by laminar boundary layer thicknesses. The latter vary with horizontal wind speed and need to be modified by surface shape factors (Burba et al., 2008). All empirical parameterizations and theoretical heat flux models within the BC framework were obtained assuming a vertical sensor placement, despite the manufacturer's recommendation of 10-15° sensor tilt to mitigate water or dust residue on the mirrors.

2.3.2. Direct path heat exchange parameterization: the "Wang" correction

Wang et al. (2017) derived a simplification of the BC approach that circumvents the underlying laminar boundary layer and surface temperature model and directly estimates the instrument path heat flux S from the ecosystem heat flux H. This is achieved by exploiting the linear relationship between H and S reported by Burba et al. (2008):

$$H = b'S - a', \quad \text{with } a' = 2.67\ (\text{W m}^{-2}),\ \text{and } b' = 0.86. \tag{6}$$

Substituting into Eq. 1 yields the instrument heating-corrected flux:

$$F_{Wang} = F_{OP} + \frac{\overline{\rho_c}}{\overline{\rho}c_p\overline{T_a}}\left(1+\mu\frac{\overline{\rho_v}}{\overline{\rho}_{dry}}\right)\left[\left(1-\frac{1}{b'}\right)H - \frac{a'}{b'}\right], \tag{7}$$

which can be expressed as a linear regression on H :

$$F_{Wang} = F_{OP} + b\,H + a, \tag{8}$$

with

$$b = \frac{\overline{\rho_c}}{\overline{\rho} c_p \overline{T_a}} \left(1 + \mu \frac{\overline{\rho_v}}{\overline{\rho_{dry}}}\right)\left(1 - \frac{1}{b'}\right), \; in\ unit, \left[\frac{s^2}{m^2}\right] \tag{9}$$

and

$$a = \frac{\overline{\rho_c}}{\overline{\rho} c_p \overline{T_a}} \left(1 + \mu \frac{\overline{\rho_v}}{\overline{\rho_{dry}}}\right) \left(1 + \mu \frac{\overline{\rho_v}}{\overline{\rho_{dry}}}\right)\left(-\frac{a'}{b'}\right), \; in\ unit \left[\frac{kg}{m^2 s}\right]. \tag{10}$$

Eq. 6 to Eq. 10 can be applied to historic datasets to obtain a CO_2 flux that is corrected for the effects of sensor surface heat exchange on the basis of co-measured sensible heat fluxes. The a' and b' coefficients originate from Burba et al. (2008) based on a 1-week experiment in the non-growing season; it is an open question whether the same coefficients can be reliably applied in other seasons and at other sites. This debate can only be resolved through direct measurements of *S*; it is not possible to derive a parameterization based on *H* during the growing season when NEE and *H* are strongly related *via* ecophysiological and physical processes.

2.3.3. Optimization via concurrent closed-path flux measurements: the "fitting" correction

An additional correction method that does not rely on temperature and heat flux models was discussed by Järvi et al. (2009) and slightly modified by Kittler et al. (2017). This correction applies a simplified calculation of S_{OP} and introduces a scaling coefficient to account for tilted sensor placement. Here, we re-evaluate their fitting method as:

$$F_{Fit} = F_{OP} + \gamma \frac{(T_S - T_a)\rho_c}{r_a (T_a + 273.15)} \left(1 + \mu \frac{\overline{\rho_v}}{\overline{\rho_{dry}}}\right), \quad with\ r_a = U u_*^2, \tag{11}$$

where γ is a unitless coefficient interpreted as the fraction of S_{op} that is being transported through the measurement cell, r_a is the aerodynamic resistance to heat transfer (s m^{-1}), ρ_c here in (μmol m^{-3}), and u_* is the friction velocity (m s^{-1}). Two parameterizations for T_S have been used in the past. The first one uses Eq. 4, whereas the second one follows a polynomial:

$$T_S = 0.0025\, T_a^2 + 0.9\, T_a + 2.07. \tag{12}$$

Here the γ and *d* parameters are estimated for night- and daytime conditions separately by non-linear least-squares optimization (initial guesses: $\gamma = 0.05$, $d_0 = 0$, $d_1 = 1$) (Järvi et al., 2009). We further evaluate the performance of the fitting correction when γ is estimated using a fixed T_S model (Eq. 12) following Kittler et al. (2017), and when parameters are optimized to minimize bias (median absolute deviation, MAD) rather than sum of squares (SS).

2.3.4. Regression and machine learning based analysis of the potential drivers of observed OP flux bias

In addition to the existing corrections above, we apply machine learning to the observed OP and CP flux differences using a variable combination of potential explanatory variables. A pre-selection of explanatory variables was performed using stepwise linear regression initiated with all variables used in the above SPHE corrections, i.e. $\overline{T_a}$, *U*, incoming shortwave- and longwave radiation fluxes, the covariances between $w' T_a'$ and $w' \rho_v'$, and the means of ρ_c, ρ_v, and T_a. We then trained an ensemble of feed-forward artificial neural networks (ANNs) to predict the OP flux bias (i.e. $F_{OP} - F_{CP}$). The most powerful set of explanatory variables was then determined based on statistical analysis against the observed $F_{OP} - F_{CP}$ data withheld from ANN training. The uniqueness of this approach lies in the flexibility of neural networks to decipher non-linear relationships and interactions between explanatory variables without prior knowledge of functional dependencies. The approach complements the stepwise linear regression analysis by strengthening our ability to identify the key explanatory variables and the likely physical drivers of $F_{OP} - F_{CP}$.

Our neural network construction follows standard community protocols (e.g. Moffat et al., 2007) and proceeds by splitting all available data into training, optimizing and validation subsamples in a repeated randomized approach using k-means clustering. Details and uncertainty inference are as described in our past work (Deventer et al., 2019).

2.4. Flux calculations and spectral corrections

Open- and closed-path fluxes were calculated, corrected, quality-controlled and filtered using the latest community protocols (Sabbatini et al., 2018). Post-processing was performed in EddyPro 7.0 (LI-COR Biosciences, Lincoln, USA). Closed-path H_2O measurements were aligned with vertical wind measurements using a relative humidity-dependent time lag optimization to compensate for H_2O adsorption/desorption on inlet tubing surfaces. Spectral corrections for high-frequency attenuation were calculated in two ways to assess the associated uncertainty: 1) using an in-situ (empirical) method (Ibrom et al., 2007; Fratini et al., 2012); and 2) using the analytical (theoretical) approach (Moncrieff et al. 1997). Attenuation due to sensor separation (crosswind and vertical separation only) were corrected following Horst and Lenschow (2009). Lastly, high-pass filtering effects due to de-trending were estimated following Moncrieff et al. (2005). For both CO_2 measurement systems the total spectral correction factors were similar, with median values of 1.11 (OP) and 1.13 (CP). The distributions of fluxes and of the OP - CP flux difference were insensitive to the choice of high frequency correction approach ($p < 0.05$, Wilcoxon Rank-Sum Test). We therefore judge spectral correction uncertainties to be negligible and use empirically-corrected fluxes for the sensor inter-comparisons that follow.

2.5. Temperature sensitivities of the LI-7500 calibration function

In this work we also characterized the LI-7500 factory calibration performance. Factory calibration follows the framework established by Welles and McDermitt (2005), with the OP analyzer measuring air mixtures of variable and known CO_2 concentrations under varying ambient temperatures ($-25°C < T_a \leq 43°C$) in a climate chamber. A 5^{th}-order polynomial is then derived fitting the measured absorptance (α) to the corresponding gas concentrations. In our analysis we evaluate this approach by quantifying the calibration fit residuals ($\delta\rho_{CO_2}$) as a function of ambient temperature at our site. Total infrared absorption in the 4.26 micron CO_2 absorption band depends not only on ρ_{CO_2}, but also on the temperature of the air mixture due to the temperature dependence of the spectral line strength and the line shape (Gordon et al., 2017). Thus, apparent changes in ρ_{CO_2} due to this $\frac{\delta\alpha}{\delta T_a}$ sensitivity can falsely be interpreted as CO_2 concentration changes; if correlated with the vertical wind these will then manifest as flux errors. Such effects are fundamentally different from the WPL dilution effects and are termed spectroscopic effects associated with absorption line broadening.

The LI-7500 internal calculation for CO_2 number density is independent of ambient temperature (Eq. 3–19 and 3–23, LI-COR Biosciences Inc 2015), corresponding to an assumption that calibration errors do not correlate with ambient temperature fluctuations. The impacts of this assumption are reduced by maintaining the critical LI-7500 optical components at constant temperature. In this study we investigate the magnitude of the LI-7500 calibration error and how it corresponds to observed flux errors relative to a closed-path system where heat-exchange related measurement errors are substantially mitigated because fluctuations in temperature are dampened by bringing the sample air to a common temperature within the sample inlet and sample cell. In the past, Bogoev et al. (2015) and Helbig et al. (2016) observed a systematic bias in the IRGASON and the EC150 with a magnitude

proportional to the sensible heat flux. They attributed the bias to the temporally inadequate spectroscopic corrections of the thermistor probe used in spectroscopic calculations.

3. Results

3.1. Plausibility of observed NEE

Between November 2018 and April 2019, the mean air temperatures at Bog Lake Peatland was −9°C, the mean soil temperatures at 10 cm depth was 1.5°C, and the albedo exceeded 0.4. Weekly photographs document a fully snow-covered vegetation canopy. Despite such photosynthetically unfavorable meteorology and phenology, we observed a strong correlation ($r^2 = 0.35$) between OP-derived NEE and H during this time, with a statistically significant ($p < 0.05$) and negative slope. For the CP analyzer, however, the NEE-H correlation was very weak ($R^2 = 0.01$) with near-zero slope (Table 1). The positive intercept in the CP NEE-H regression suggests ongoing microbial CO_2 respiration in winter, even during nighttime, which can be explained by above-zero soil temperatures (insulated from freezing air temperatures by snow). The observed baseline respiration (0.3 μmol m^{-2} s^{-1}) agrees well with observations from flux chamber measurements made at SPRUCE (Hanson et al., 2016).

In contrast, OP NEE-H regression results suggest net CO_2 uptake at near-zero values of H, and increasing net CO_2 uptake during winter daytime with increasing H. Based on the local meteorological and phenological conditions we consider these fluxes to be physically unrealistic. Any systematic errors (excluding differences between OP vs. CP measurement principles) inherent in the EC application or site-specific violation of EC theory should be common to both the OP and CP fluxes as measurement height and sonic measurements were identical.

Observed OP - CP differences are thus assumed hereafter to reflect biases in the OP measurements or in their associated flux calculations. In the following, we examine the magnitude of this bias, its persistence throughout both cold and warm seasons, and its sensitivity to different sensor-surface path heat exchange corrections.

3.2. NEE bias

The concurrent CO_2 flux measurements reveal a persistent OP *vs.* CP NEE bias ($\Delta\ NEE = F_{OP} - F_{CP}$) (Fig. 1). Values of Δ NEE follow a double exponential distribution skewed towards negative values; this OP tendency towards smaller-magnitude upward fluxes and/or larger-magnitude downward fluxes manifested during the winter as well as during the growing seasons (Fig 1b, c). The median Δ NEE value was −0.4 μmol m^{-2} s^{-1} with an inter-quartile range (IQR) of −0.9 to −0.1 μmol m^{-2} s^{-1}.

The Δ NEE magnitude exhibited temporal variability at our site. In the growing season during daytime (albedo < 0.4; global radiation > 20 W m^{-2}), the median fractional bias ($\frac{\Delta NEE}{|F_{cp}|}$) was approximately 30% (−0.36 μmol m^{-2} s^{-1}). At night, biases were smaller (~14%, −0.20 μmol m^{-2} s^{-1}). During the snow-covered season, biases became much larger (median ≈ 150%, −0.46 μmol m^{-2} s^{-1}) with less systematic difference between day- and nighttime conditions. For the snow-covered season the default OP fluxes implied (on average) net CO_2 uptake with a maximum around noon, whereas CP fluxes showed a relatively steady release of CO_2 throughout the day (Fig. 1b). During the growing season the OP system measured larger net daytime CO_2 uptake than did the CP sensor, with the OP and CP CO_2 fluxes tending to converge at night (Fig. 1c).

Table 1
Orthogonal regression statistics between sensible heat fluxes and NEE.

Analyzer	Coefficient	95% Confidence Limits	
		lower	upper
	slope [(μmol m^{-2} s^{-1})/(W m^{-2})]		
7200	−0.003	−0.005	−0.001
7500A	−0.023	−0.024	−0.022
	intercept [μmol m^{-2} s^{-1}]		
7200	0.324	0.307	0.342
7500A	−0.345	−0.366	−0.323

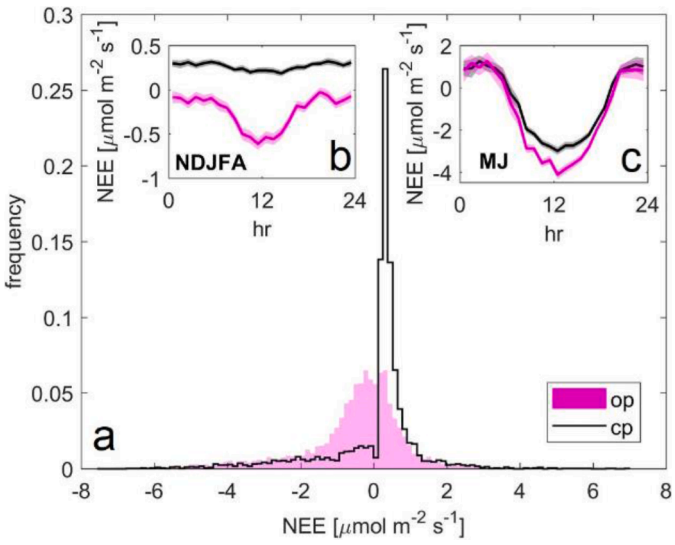

Fig. 1. (a) Histograms of CO_2 fluxes measured with open- (purple) and closed-path (black) analyzers from November 2018 through June 2019 (mean T_a = −3.7°C). Panels inset show median hourly fluxes (lines) with standard errors (shaded areas) for (b) November 2018 through April 2019 and (c) May 2019 through June 2019.

3.3. Relation of NEE bias to environmental conditions

The largest Δ NEE episodes in this study were observed during periods of largely positive ecosystem heat fluxes ($p < 0.01$, $R^2 = 0.12$), with larger negative OP biases associated with upward heat fluxes (Fig. 2a). This relationship was most evident in the snow covered season ($\Delta\ NEE = -26.3\ \overline{w'T_a'} - 0.71$), but was also significant in the growing season ($\Delta\ NEE = -4.1\ \overline{w'T_a'} - 0.31$) as seen in Fig. 1c. In contrast, Δ NEE values showed no significant relationship with horizontal wind speed ($p = 0.11$, $R^2 = 0.00$) or with ambient temperatures on either weekly ($p = 0.65$, $R^2 = -0.03$) or 30-min ($p = 0.165$, $R^2 = 0.00$) timescales (Fig. 2b). When dividing Δ NEE by the CP flux it becomes apparent that the largest fractional biases occurred under near-zero ecosystem heat fluxes and cold air temperatures ($p < 0.01$, $R^2 = 0.5$).

The negative Δ NEE:$\overline{w'T_a'}$ intercept for all seasons (Fig. 2a) reveals the presence of a residual OP bias that is independent of ecosystem heat fluxes, suggesting increased SPHE due to OP sensor self-heating. However, we find no significant differences in the ΔNEE : $\overline{w'T_a'}$ regression coefficients under varying degrees of turbulence (all data, $u_* > 0.2$, and $u_* > 0.35$). Thus, while the OP measurement biases scale with heat fluxes, they are independent of turbulence, suggesting that SPHE is not the only reason for OP CO_2 flux bias.

In addition to the above single-variable regression analyses, we performed multiple (stepwise) linear regressions (SLR) to test the degree to which a combination of explanatory variables could improve upon a model based on heat fluxes alone. We find that additional statistical power is provided by (in descending order of F statistics): $\overline{w'T_a'}$, $\overline{T_a}$, $\overline{\rho_c}$, $\overline{\rho_v}$, $\overline{w'\rho_v'}$, and longwave radiation fluxes. Non-significant contributions ($p > 0.05$) were found for wind speed and shortwave radiation fluxes (Table 2). ANNs trained on combinations of the above variables confirm

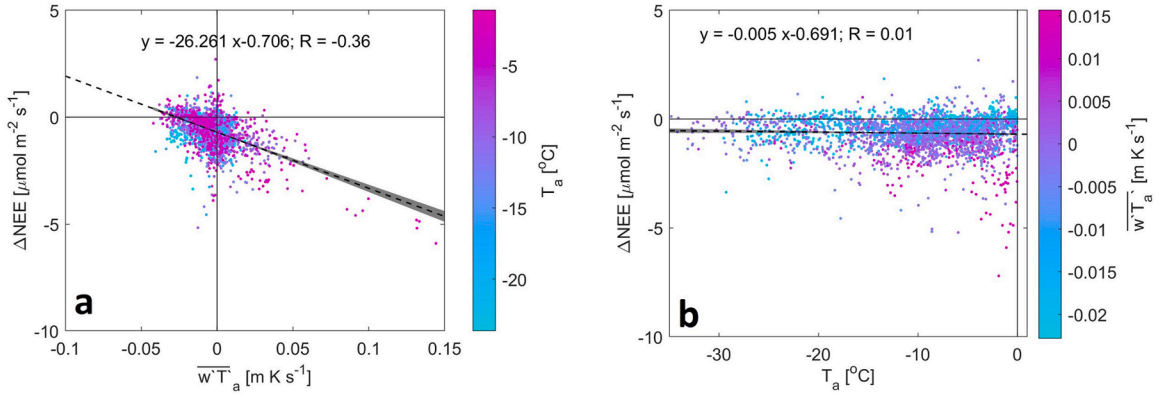

Fig. 2. Relationship between absolute flux bias (Δ NEE = $F_{OP} - F_{CP}$), kinematic heat flux ($\overline{w'T_a'}$), and ambient temperatures (T_a). Data plotted (n = 3061) are for the snow-covered season (albedo > 0.4) when $T_a < 0$ °C. Dashed lines and equations represent ordinary least squares regressions with 95% confidence intervals in shaded gray.

Table 2
The relation between observed OP-CP flux differences and auxiliary variables. The top part of the table summarizes stepwise linear regression analyses. The bottom panel summarizes the root mean square error and correlation coefficients between reference CP fluxes and OP fluxes after flux bias was predicted using artificial neural networks (ANN) that were trained based on explanatory data combinations, that either excluded H_2O terms*, or excluded temperature terms**.

Variable	sum of squares	sum of squares/df	F	p-value
$\overline{w'T_a'}$	255.3	255.3	243.8	5.40E-54
$\overline{T_a}$	150.1	150.1	143.3	1.10E-32
$\overline{\rho_c}$	68.1	68.1	65	8.80E-16
$\overline{\rho_v}$	66.4	66.4	63.5	1.90E-15
$\overline{w'\rho_v'}$	25.5	25.5	24.3	8.30E-07
net longwave radiation	4.8	4.8	4.6	3.20E-02
Statistic	F_{OP_ANN}	F_{OP_ANN} (w/o H_2O)	F_{OP_ANN} (w/o temperature)	F_{OP}
RMSD (F_{OP_ANN}, F_{CP})	0.88	0.90	1.04	1.10
R (F_{OP_ANN}, F_{CP})	0.93	0.92	0.90	0.89
R (Δ (F_{OP_ANN}-F_{CP}), Δ (F_{OP}-F_{CP}))	0.50	0.47	0.31	n/a

* $\overline{w'\rho_v'}$ and $\overline{\rho_v}$
** $\overline{w'T_a'}$ and $\overline{T_a}$

the overpowering importance of temperature terms (in particular the kinematic heat flux) in explaining the observed Δ NEE (Table 2). The SLR and ANN analyses both show that the inclusion of water vapor terms adds explanatory power to the models/networks ($p < 0.05$). This points towards previously identified CO_2 measurement biases associated with line broadening effects and direct absorption interference from water vapor (Welles and McDermitt 2005; Kondo et al., 2014). It thus appears that, in addition to SPHE, OP NEE biases may arise from incomplete spectroscopic corrections.

Overall, we find only weak evidence for the Δ NEE dependence on environmental conditions proposed by Burba et al. (2008), indicating that SPHE theory alone is insufficient to explain OP measurement bias. In the following, we quantify the OP instrument surface temperatures and analyzer path heat fluxes and assess the degree to which they co-vary with ambient temperatures and ecosystem heat fluxes.

3.4. The extent and variability of OP surface heating

Instrument surface temperature measurements allow us to quantify OP surface heating and assess the representativeness of the temperature models presented in Burba et al. (2008). Our bottom-surface temperature observations follow the trends observed in Burba et al. (2008), namely: (i) surface temperatures varied near-linearly with ambient temperatures; (ii) bottom-surface temperatures nearly always exceeded ambient temperatures during both day and night; and (iii) this offset was enhanced at night and at low temperatures (Fig. 3). The top-surface temperatures agreed well with the Burba model at night but exhibited a much larger-than-predicted enhancement during daytime. Overall, the T_s vs. T_a regression parameters estimated here diverge from those of Burba et al. (2008) (Table 3), suggesting that these coefficients are site-specific (e.g. our OP tilt angle was ~40° *vs.* near-vertical alignment in Burba et al. (2008)), rather than constants that can be applied universally.

Burba et al. (2008) noted that instrument surface temperatures are likely to vary between sites due to tower- and sensor-placement specific influences from shading, sun angle, and wind distributions. The aerodynamic resistance to heat transfer decays approximately exponentially with wind speed. Thus, at low wind speeds surface temperatures can increase due to suppressed heat exchange and air parcel transport. In Table 3 and below we examine uncertainties in the surface temperature model; these will later be propagated into the SLR correction to estimate its sensitivity to the parameter estimates from Table 3.

3.5. Relationship between sensor path heat exchange and ecosystem heat fluxes

Fig. 4 shows that heat fluxes measured close to the OP measurement path (S) differ from the true ecosystem heat fluxes (H), especially under weakly established turbulence. In particular, S measured near the bottom exceeded ambient heat fluxes measured by the sonic anemometer ($H = 0.84\ S + 13$ W m^{-2}), with a mean bias error of 16.1 W m^{-2}. For comparison, Burba et al. (2008) reported a similar slope (0.86), but a smaller intercept (2.67 W m^{-2}) for their measurements over a clear-cut forest. We find here that the S -H differences become smaller (minimum

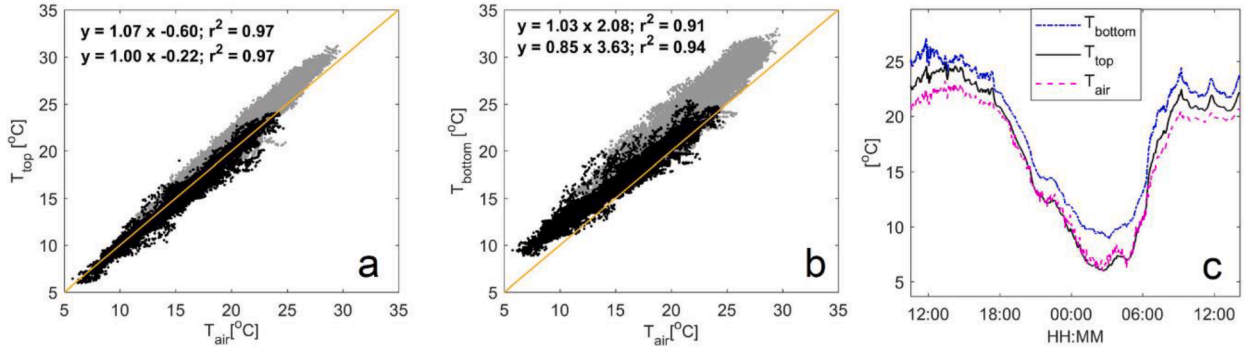

Fig. 3. Scatterplot (n > 30,000) of ambient vs. LI-7500A surface temperatures. Surface temperatures were measured in close proximity to the top (panel a) and bottom (panel b) windows; data shown are separated into nighttime (black dots) and daytime (gray dots) with the 1:1 relation in yellow. Panel c shows an example 24-hour period (noon to noon, June 20th/21st 2019) with a large ambient temperature amplitude during mostly clear-sky conditions. Lines denote temperature measurements near the bottom window (blue dash dotted), the top mirror (black solid) and in ambient air (magenta dashed).

Table 3
Coefficients from regression analysis of ambient vs. sensor surface temperatures[a].

	top		bottom	
	slope (°C/°C)	Intercept (°C)	slope (°C/°C)	intercept (°C)
Daytime				
This study	1.07 [1.06; 1.11]	−0.60 [−0.69; −0.58]	1.03 [1.00; 1.06]	2.08 [2.05; 2.23]
Burba et al. (2008)	1.01	0.24	0.94	2.57
Nighttime				
This study	1.00 [0.98; 1.01]	−0.22 [−0.23; −0.21]	0.85 [0.83; 0.88]	3.63 [3.60; 3.73]
Burba et al. (2008)	1.01	−0.41	0.83	2.17

[a] values in brackets indicate the 95% confidence intervals.

of 9.0 W m^{-2}) and the $S(H)$ regression becomes more linear with slopes close to unity for $u_* > 0.35$ m s^{-1} (Fig. 4c). During our study, S measured near the top yielded much smaller and on average negative (i.e. cooling) deviations from H, with a mean bias error of 1.1 W m^{-2} and $H = 1.36\ S - 2$ W m^{-2}. These results indicate that S_{bot} is partly offset by S_{top} . Seasonal analysis our S measurements as functions of H reveal that the heat source from the bottom of the instrument is particularly large in winter, and that the cooling from the top of the instrument is particularly large in summer (as compared to H) (Table 4). When averaging our two S measurements to estimate OP representative S, we find a weak relationship with T_a ($R^2 = 0.002$; RMSD = 19.1 W m^{-2}; $p < 0.01$). Stepwise linear regression yields best predictions using a 2-term model using shortwave incoming radiation and U but yields negligible improvement in predictive power ($R^2 = 0.09$; RMSD = 17.9 W m^{-2}; $p < 0.01$) over the simple linear regression above, suggesting that seasonality in S-H is complex, complicating a robust parameterization of $S(H)$.

If the observed NEE bias is caused by OP surface heat exchange, we expect to find a relationship between ΔNEE and $S - H$. Here we observe only a very weak positive relationship between flux bias and $S - H$, both on an absolute (ΔNEE; $p < 0.01$, $R^2 = 0.01$) and normalized ($\Delta NEE / |F_{cp}|$; $p < 0.01$, $R^2 = 0.01$) basis, suggesting that (within the uncertainty of our S measurements) $S - H$ does not in fact drive variability in ΔNEE. The sensor heating theory posits that the surface: ambient temperature gradient causes additional heat fluxes in the OP measurement path leading to air density fluctuations not accounted for in the traditional WPL terms. Properly accounting for S should in that case reduce the bias between OP and CP flux measurements. If, on the other hand, other sources of OP flux bias persist (e.g. inadequate spectroscopic corrections) an SPHE-based dilution correction will be unsuccessful in eliminating ΔNEE. In the following, we evaluate each of the SPHE corrections outlined in section 2.3 in terms of their performance in reducing the ΔNEE observed in this study.

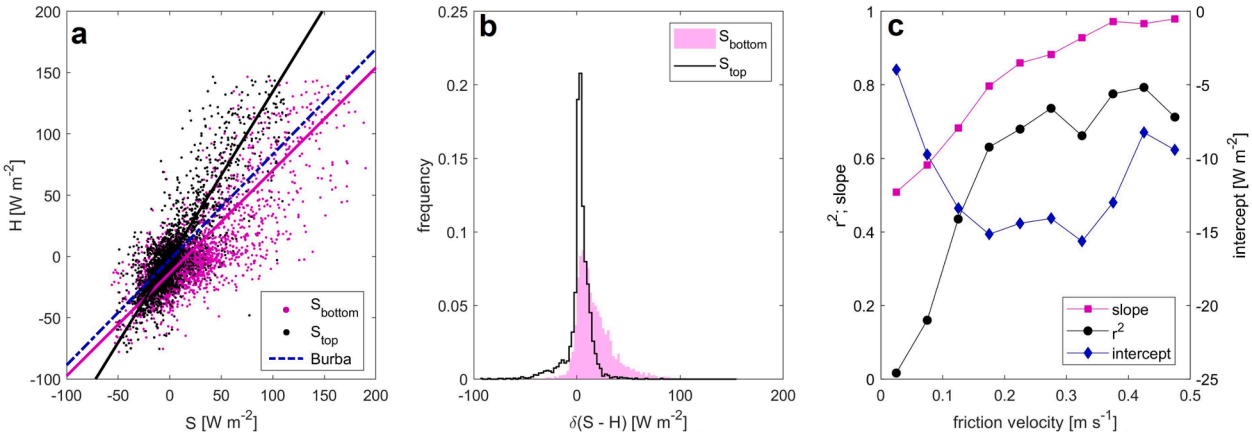

Fig. 4. Panel a shows scatter plots of ecosystem heat fluxes (H) vs. heat fluxes measured close to the open-path windows (S) for the top surface (black) and bottom surface (magenta) with orthogonal regression lines. Also shown (blue line) are the regression results of Burba et al. (2008) which represent path-averaged heat flux measurements. Panel b shows the frequency distributions of the differences between OP and ecosystem heat fluxes measured. Panel c shows orthogonal regression statistics for S_{bottom} vs. H binned into 0.05 m s^{-1} friction velocity classes.

Table 4
Geometric regression estimates of SPHE as a function of ecosystem heat fluxes (H) with 95% confidence intervals in parenthesis. SPHE was measured near the top (S_{top}), and near the bottom (S_{bot}) of the LI-7500A analyzer.

	S_{bot}*		S_{top}*		mean(S_{bot}*,S_{top}*)	
	intercept	slope	intercept	slope	intercept	slope
day snow	21.1 (20.2, 21.9)	1.65 (1.56, 1.75)	2.7 (2.3, 3.2)	0.94 (0.89, 1.0)	9.9 (9.4, 10.4)	1.07 (1.02, 1.13)
day green	19.3 (17.1, 21.5)	1.09 (1.04, 1.15)	−0.25 (−1.5, 0.99)	0.73 (0.7, 0.75)	10.9 (9.3, 12.5)	0.89 (0.85, 0.93)
night snow	15.0 (14.3, 15.6)	1.19 (1.13, 1.25)	1.6 (1.3, 0.7)	0.70 (0.66, 0.71)	7.0 (6.6, 7.4)	0.83 (0.79, 0.87)
night green	16.0 (14.95, 16.97)	1.17 (1.05, 1.29)	1.0 (0.5, 1.4)	0.64 (0.58, 0.69)	8.0 (7.3, 8.7)	0.84 (0.76, 0.91)

* here S_{bot} and S_{top} represent the measured heat flux in the LI-7500 path near the bottom or top mirror of the analyzer, and not just the heat emitted from the analyzer surfaces alone.

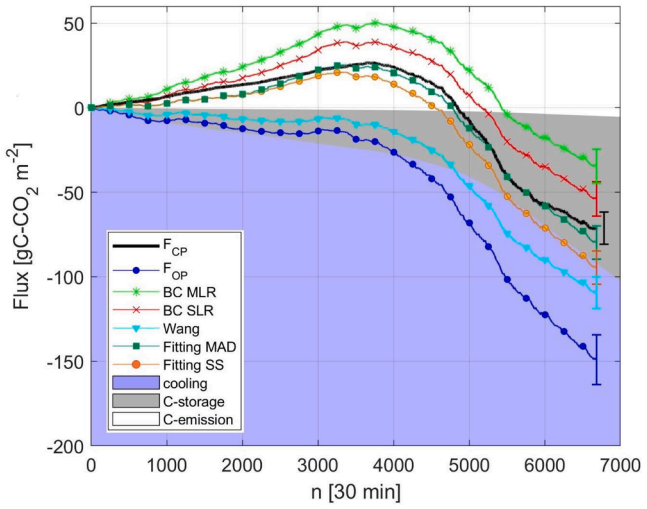

Fig. 5. Cumulative time series for default calculated (blue) and sensor-path heat exchange (SPHE)-corrected open-path (OP) NEE estimates (BC SLR – red with crosses, BC MLR – green with asterisks, Wang – cyan with triangles, Fitting optimized for MAD – dark green with squares, Fitting optimized for SS – orange with circles). Also shown is the reference closed-path NEE estimate (thick black line). Error bars denote the cumulative flux random errors in each case (Finkelstein and Sims, 2001). The error bar of the reference flux is offset to the right for easier comparison. The graph background is color coded into C-emitting, C-storing, and cooling regimes as discussed in-text.

3.6. Cumulative fluxes

Quantification of OP biases is essential when deriving carbon and radiative forcing budgets used for global syntheses and model evaluations. As a first benchmark for the various OP corrections above, we compare the cumulative NEE budget in each case with the corresponding reference CP NEE budget (Fig. 5, Table 5). While the CP measurements yield a cumulative (non-gap-filled, n = 6681) flux of −71.3 gC-CO_2 m^{-2}, the default OP fluxes imply a much larger sink of −149.1 gC-CO_2 m^{-2}—a bias of −77.8 gC-CO_2 m^{-2}, or 110% of the CP value. During the snow-covered season, these two time series diverge with apparent net CO_2 uptake in the default F_{OP} timeseries versus a steady increase in the cumulative F_{CP} values. Finally, although the CP- and default OP-based cumulative NEE time series both decrease during the growing season, the CO_2 uptake rate inferred from the default OP dataset is larger, thus further exacerbating the NEE bias accrued during the snow-covered season. Cumulative flux differences between the default F_{OP} and reference F_{CP} are much larger than the respective flux random errors (Table 5).

Each of the SPHE corrections decreases the inferred OP sink strength and hence the bias against the cumulative reference fluxes (Table 5). Among them, the MLR and Wang methods respectively introduced the largest (147%) and smallest (51%) corrections relative to the observed $F_{OP} - F_{CP}$ bias. Overall, the best agreement in terms of the cumulative $F_{OP} - F_{CP}$ flux difference was found for the Fitting method when optimized for MAD (−8.4 gC-CO_2 m^{-2}), and for the BC SLR method (17.4 gC-CO_2 m^{-2}). Of all investigated correction approaches, only these two yield cumulative fluxes within the uncertainty of the reference dataset (Fig. 5, Table 5). Less accurate results were obtained from (in ascending order of bias): the BC MLR method, the Fitting method when optimized for SS, and the Wang method.

Table 5 and Fig. 5 show that one's choice of OP correction approach can change not only the magnitude but also the sign of the derived ecosystem C-balance and net radiative forcing. To illustrate this, we compare the range of OP NEE corrections to the wetland's methane budget derived *via* concurrent CH_4 EC measurements. At the end of our measurement period, the maximum discrepancy between cumulative OP NEE estimates was ≈115 gC m^{-2}—greater than the threshold at which the ecosystem switches between net positive and negative radiative forcing (based on a 100 year forcing-neutral flux ratio of −19.2 $\frac{gC-CO_2}{gC-CH_4}$ (Petrescu et al., 2015)). Seasonally, the default OP fluxes, SPHE-corrected OP fluxes, and reference CP fluxes fall into 3 different regimes: C-emitting, C-storing, and cooling, with the latter indicating net C storage sufficient to offset the radiative forcing of the wetland's CH_4 emissions. Such NEE uncertainties diminish our confidence in the radiative forcing budget of wetland sites; a better constraint on OP flux

Table 5
Carbon flux budgets from all deployed analyzers and all evaluated SPHE correction methods.

	cumulative flux ± random error	$\Delta F_{OP} - F_{CP}$	correction	correction relative to ($F_{OP} - F_{CP}$)
	gC-CO_2 m^{-2}	gC-CO_2 m^{-2}	gC-CO_2 m^{-2}	%
F_{CP}	−71.3 ± 9.5			
F_{OP}	−149.1 ± 14.8	−77.8		
BC SLR	−53.9 ± 10.0	17.4	95.2	122
BC MLR	−34.5 ± 10.1	36.8	114.6	147
BC with measured S	−87.1 ± 9.5	−15.8	62.0	83
Wang	−109.4 ± 9.5	−38.1	39.7	51
Fitting MAD	−79.7 ± 9.8	−8.4	69.4	89
Fitting SS	−94.62 ± 9.9	−23.3	54.5	70
CH_4	4.83 ± 0.9 gC-CH_4			

Table 6
Taylor diagram statistics of regression analysis between the reference NEE and the various corrected open-path flux estimates.

	reference F_{CP}	default F_{OP}	BC MLR	BC SLR	Wang	Fitting MAD	Fitting SS
NEE mean (μmol m^{-2} s^{-1})	−0.49	−1.03	−0.24	−0.37	−0.76	−0.55	−0.65
NEE standard deviation (μmol m^{-2} s^{-1})	2.34	2.38	2.30	2.30	2.14	2.37	2.39
RMSE (μmol m^{-2} s^{-1})		1.10	1.08	1.10	1.08	1.20	1.08
correlation coefficient		0.89	0.89	0.89	0.89	0.88	0.89
bias error		−0.54	0.25	0.12	−0.26	−0.06	−0.16
slope x = H *; y = NEE (μmol m^{-2} s^{-1}/W m^{-2})	−0.003	−0.023	−0.016	−0.019	−0.014	−0.017	−0.018
slope x = F_{CP}; y = F_{OP}		1.13	0.98	0.98	1.02	0.98	0.98

* orthogonal regression estimates for a period with Albedo > 0.4 and mean $T_a = -9°C$; $n = 3673$

biases is critical to better constrain these budgets.

3.7. Correlation statistics of 30 min fluxes

In addition to evaluating the OP correction approaches based on the resulting cumulative fluxes, we examine here their correlation statistics with respect to the reference CP fluxes on a 30-min timescale. Table 6 shows that none of the evaluated corrections significantly improve the correlation coefficients and RMSE over the default OP fluxes. All investigated approaches yielded an $F_{OP} : F_{CP}$ regression slope close to 1.0 (± 0.03). As expected, the Fitting (optimized for MAD) method was most successful in minimizing bias errors, followed by the SLR method. The Wang approach suppressed the flux standard deviation below that of the reference, and it most strongly reduced the spurious cold-season $F_{OP} : H$ slope (section 3.1.). However, none of the corrected $F_{OP} : H$ slope estimates fall within a factor of 4 of the reference value. Based on this finding it is insufficient to constrain OP flux bias solely based on SPHE theory.

In the following we explore in detail the relevant error sources for each SPHE OP flux correction method.

3.8. Evaluation of the Burba corrections

When considering historic OP datasets without available reference flux measurements, a key question arises: How representative are the Burba et al. (2008) parameterizations for EC stations with variable tower designs and sensor tilt?

To evaluate the sensitivity of the BC approach to the model temperature coefficients, we propagate the uncertainties associated with our measured surface and ambient temperatures (section 3.4) into the cumulative flux time series. Specifically, we randomly resample ($n = 1000$) each temperature coefficient within its 95% confidence interval (Table 3) and obtained minimum and maximum cumulative F_{OP} corrections of 111 gC m^{-2} and 131 gC m^{-2}, respectively. The resulting sensitivity index $\left(\frac{max-min}{mean}\right)$ is ~17% (20 gC m^{-2}), or 25% of the bias between the default OP and reference CP fluxes (Table 5). This 17% uncertainty arises solely from the 95% confidence interval of the SLR surface temperature model. Additional and likely larger uncertainties for the BC approach stem from radiation and wind speed parameter uncertainties (in the case of MLR) and from assumptions of vertical heat transfer through the measurement path (in the case of tilted sensors). Burba et al. (2008) did not provide uncertainties for their boundary layer, temperature, or heat flux models, preventing any direct uncertainty inference. However, from Fig. 2 and 3 in Burba et al. (2008) the scatter around their fitted temperature models is similar to that found here, so that our error analysis above is likely a fair representation.

The SLR and MLR methods share identical surface boundary layer and surface heat flux formulations; differences between these corrections thus arise solely from the instrument surface temperature parameterizations. We find here that: (i) for a given radiation flux $S_{S,MLR}$ and $S_{S,SLR}$ diverge as a function of wind speed (Fig. 6a); (ii) in our study the SLR correction is systematically less than the MLR correction for wind speeds < 3 m s^{-1} and (iii) this relation is reversed at higher wind speeds (Fig. 6b). Together, these observations explain the cumulative difference between MLR- and SLR-corrected fluxes found above (Fig. 5). We find that the cumulative SLR-corrected OP fluxes agree more closely with the reference CP fluxes than do the MLR results (Fig. 5), with MLR corrected OP fluxes higher ($p < 0.05$) than the SLR-corrected fluxes by 0.13 μmol m^{-2} s^{-1}.

When applying the BC with directly measured S (Eq. 2) corrected cumulative OP fluxes fall within the uncertainty of the reference fluxes

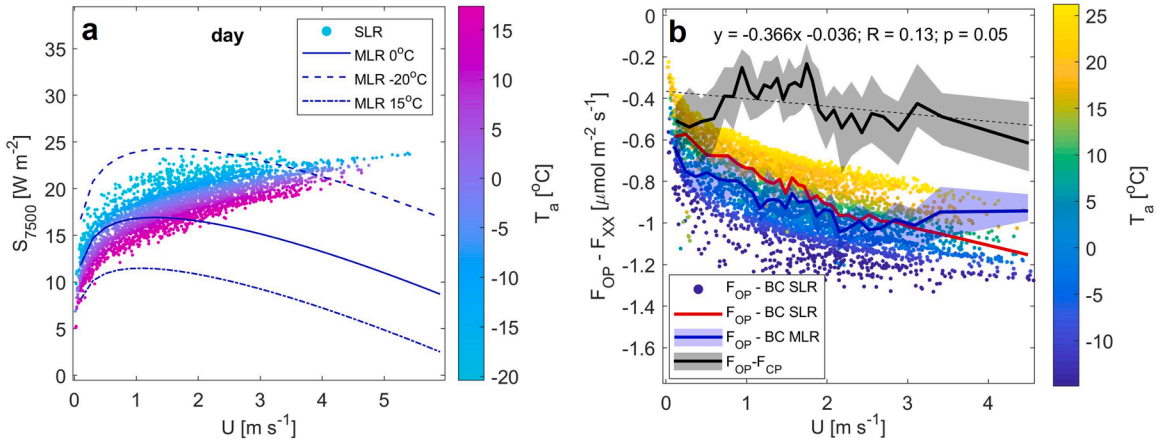

Fig. 6. Panel a shows calculated instrument surface heat fluxes (S_{7500}) for the BC SLR method (dots, color mapped by air temperature) and for the BC MLR method (lines). The latter were calculated for a radiation flux of 150 W m^{-2} and for 3 different ambient temperatures. Panel b shows the differences between traditionally calculated F_{OP} to BC corrected fluxes as well as the difference to the closed-path (CP) reference flux as a function of wind speed. Lines show median values for n = 30 wind speed bins chosen to encompass equal number of flux differences. Shaded areas show the IQR of each bin. Dots show 30-min differences (F_{OP} – BC SLR) heat-mapped by ambient temperature. Also shown is the orthogonal regression (dashed black line) for the F_{OP} - F_{CP} relation with wind speed.

Table 7
Taylor diagram statistics of regression analysis between the reference NEE, default F_{OP} and F_{OP} corrected using BC with either directly measured S or modeled S. This analysis was performed for a subset of the dataset, where S was directly measured near the top (S_{top}) and bottom (S_{bot}) of the OP analyzer (n = 2391).

	reference F_{CP}	default F_{OP}	BC S from S_{bot}	BC S from S_{top}	BC S from mean(S_{bot}, S_{top})	BC S from SLR
NEE mean (μmol m^{-2} s^{-1})	−0.13	−0.64	0.27	−0.62	−0.17	0.10
NEE standard deviation (μmol m^{-2} s^{-1})	1.49	1.64	2.06	2.28	2.08	1.44
RMSE (μmol m^{-2} s^{-1})	0.00	0.78	1.46	1.33	1.24	0.83
correlation coefficient	1.00	0.88	0.70	0.83	0.81	0.83
bias error	0.00	−0.51	0.40	−0.49	−0.05	0.13
slope x = H *; y = NEE (μmol m^{-2} s^{-1}/W m^{-2})	−0.004	−0.020	−0.031	−0.045	−0.025	−0.045
slope x = F_{CP}; y = F_{OP}		1.12	1.12	1.08	1.16	1.08

* orthogonal regression estimates for a period with Albedo > 0.4 and mean $T_a = -9$°C;

(mean bias error = 0.05 μmol m^{-2} s^{-1}). However, this cumulative agreement does not manifest in regression statistics of 30-min fluxes. We observe that OP fluxes corrected with BC using measured S yield worse forecasting statistics against F_{CP} as compared to the default F_{OP} or F_{OP} corrected with BC SLR (Table 7).

3.9. Evaluation of the Wang correction

We next investigate the degree to which bias in OP-derived NEE estimates can be corrected solely on the basis of collocated sensible heat flux measurements. Applying Eq. 9 and 10 to our observations yields coefficients (median with IQR) of $a = -0.17$ (0.004) μmol m^{-2} s^{-1} and $b = -0.009$ (0.001) (μmol m^{-2} s^{-1})/(W m^{-2}). For comparison, Wang et al. (2017) reported mean coefficients across 64 FLUXNET sites of $a = 0.02$ $\mu mol\ m^{-2}\ s^{-1}$ and $b = -0.008$ (μmol m^{-2} s^{-1})/(W m^{-2}).

When we estimate a and b directly from the observed relationship between H, S and F_{OP} *via* directly measured instrument-path heat fluxes (Eq. 2) rather than using Eq. 9 and Eq. 10 with default values for a' and b', the resulting coefficients are significantly larger: $a = -0.34$ μmol m^{-2} s^{-1}; $b = -0.023$ (μmol m^{-2} s^{-1})/(W m^{-2}). These values fall at the upper end of the coefficients presented in the Wang et al. (2017) meta-analysis (which were not obtained from direct measurements). This discrepancy between the calculated and parameterized a and b coefficients is due to the a' and b' constants in Eq. 7-10, which are from Burba et al. (2008) and not representative for our study site (section 3.4 and 3.5). Direct estimation of a and b is thus recommended.

3.10. Evaluation of the Fitting method

We find that the Fitting approach does not appreciably improve the linearity between the corrected OP and reference CP fluxes. For example, $F_{OP} : F_{CP}$ correlation coefficients remained unchanged at 0.89 when minimizing the sum of squares. Kittler at al. (2017) likewise reported minimal improvement in correlation coefficients (from 0.96 to 0.97 during daytime, and from 0.81 to 0.82 during nighttime) when applying the same approach. When the Fitting corrections are performed based on median absolute deviation (MAD), cumulative Δ NEE is reduced from 23.3 to 8.4 gC-CO_2 m^{-2}, i.e. to within the uncertainty of the reference flux (Table 5). The use of MAD optimization, however, increases the RMSE above that of the default F_{OP} (Table 6).

A cross-study comparison of γ estimates (Eq. 11; Table 8) suggests that 6% to 18% (during daytime) and 4 to 9% (during nighttime) of heat from sensor surfaces is transported through the measurement path. A larger degree of variability is observed for the temperature coefficient d (Table 8). Our γ and d estimates differ from those of Järvi et al. (2009), but are close to those of Kittler et al. (2017) who reported variability in γ as a function of wind speed and wind direction. We thus expect differing sensor orientation, tower design, and site climatology to cause variability in γ and d between sites and studies.

We find here that the Fitting approach under-corrects the cumulative Δ NEE by 52.0, 28.1, and 24.7 gC-CO_2 m^{-2} when using coefficients from Järvi et al. (2009) (urban site), Järvi et al. (2009) (forest site), and Kittler et al. (2017), respectively. All 3 corrections thus yield a larger NEE bias than the universal BC SLR approach (17.4 gC-CO_2 m^{-2} over-correction). Furthermore, the 3 Fitting corrections above yield respective $F_{OP} : F_{CP}$ RMSE values of 1.09, 1.15, and 1.08 μmol m^{-2} s^{-1}, similar or slightly worse than the result obtained for BC SLR (1.08 μmol m^{-2} s^{-1}).

3.11. Temperature sensitivities of the LI-7500 calibration

To quantitatively assess the temperature sensitivity of the LI-7500 response we characterized its factory calibration performance under

Table 8
Optimization results for the parameters γ (fraction of heat transported through the sensor path, d_1 (slope for the $T_s : T_a$ regression), and d_0 (intercept for the $T_s : T_a$ regression) used in Eqs. 10a and 10b, separated by day- and nighttime conditions.

		γ	d_1	d_0
		(dimensionless)	slope (°C/°C)	intercept (°C)
T_s from Eq. 10a				
this study	day	0.180 ± 0.024	0.98 ± 0.002	1.43 ± 0.112
Järvi et al. (2009), urban	day	0.060 ± 0.011	1.14 ± 0.010	1.77 ± 0.070
Järvi et al. (2009), forest	day	0.085 ± 0.003	0.93 ± 0.010	3.17 ± 0.170
this study	night	0.062 ± 0.008	0.89 ± 0.014	2.93 ± 0.129
Järvi et al. (2009), urban	night	0.060 ± 0.011	1.13 ± 0.010	−0.38 ± 0.040
Järvi et al. (2009), forest	night	0.085 ± 0.003	1.05 ± 0.020	1.52 ± 0.140
T_s from Eq. 10b				
this study	day	0.098 ± 0.0024		
Kittler et al. (2017)	day	0.130 ± 0.0040		
this study	night	0.067 ± 0.0017		
Kittler et al. (2017)	night	0.042 ± 0.0030		

Coefficients are shown ± 1 standard deviation from repeated optimizations based on 100 subsamples randomly drawn out of 75% of all data.

varying ambient temperatures (Fig. 8). We find here that the calibration fit residuals scale with ambient temperature and that this relation ($\frac{\delta\rho_{CO_2}}{\delta T_a}$) is not constant over the range of analyzed CO_2 concentrations (0 ppm $\leq \chi_{CO_2} \leq$ 2981 ppm). The potential flux error associated with this temperature sensitivity is additive and proportional to SPHE: $\delta F_{op} = \frac{\delta\rho_{CO_2}}{\delta T_a} \cdot \overline{w' T_a'}$.

The temperature sensitivity of the calibration residuals can be as large as 0.009 mmol m^{-3} K^{-1} at ambient CO_2 levels (396 ppm $\leq \chi_{CO_2} \leq$ 505 ppm), with positive residuals for $T_a > 10$ °C and negative residuals for cooler temperatures (Fig. 8b). For comparison, kinematic heat fluxes range from −0.1 m K s^{-1} to 0.2 m K s^{-1} at our site, corresponding to flux errors ranging from −0.9 to 1.8 μmol m^{-2} s^{-1} (in the context of a median observed OP-CP bias was 0.54 μmol m^{-2} s^{-1}).

4. Discussion

We find substantial differences between OP and CP CO_2 flux measurements. To test the plausibility of the two sets of NEE observations we investigated the relationship between cold-season CO_2 fluxes and ecosystem sensible heat fluxes (*H*). Based on vegetation phenology and physiology, no such relationship is expected for our site. Nevertheless, near-linear NEE-*H* relationships have been reported during winter for many FLUXNET sites (Helbig et al., 2016; Wang et al., 2017), with apparent CO_2 uptake increasing linearly with increasing energy fluxes. In the absence of instrumental artifacts or violation of eddy-covariance assumptions (e.g. flux-footprint homogeneity, stationarity), such a relationship would imply either photosynthetic activity or a temperature/radiation dependence for other CO_2 sinks (e.g. a chemical sink in the soil). Incubations in large-collar chambers at the nearby (<3 km distance) Spruce and Peatland Responses Under Changing Environments (SPRUCE) site (Hanson et al., 2016) show that a dominant soil sink can be ruled out for our site, as the CO_2 efflux at SPRUCE remained positive (averaging 0.4 μmol m^{-2} s^{-1}) at near-zero soil temperatures. At Bog Lake Peatland, OP flux measurements under analogous conditions exhibited significant correlations with ecosystem heat fluxes. This supports our contention that the OP-CP flux differences are due to OP measurement artifacts. While similar OP biases were previously noted in the cold season, we show here that they persist into the growing season and are thus a year-round concern.

Our measurements reveal significant temperature gradients between OP analyzer surfaces and ambient air, leading to divergent SPHE versus ecosystem heat fluxes. While this is consistent with the idea that sensor path heat exchange drives OP biases (Burba et al., 2008), we find only weak relationships between these biases and the analyzer-to-ambient temperature or heat flux gradients. We observe a relationship between OP bias and sensible heat fluxes that is inconsistent with SPHE theory. We identify several shortcommings in previous correction approaches:

Our results cast doubt on the argument that the BC are universally applicable. Järvi et al. (2009) report under-corrections for both approaches, whereas we find that both lead to flux over-corrections. However, our results are consistent with Järvi et al. (2009), in showing that the SLR method yields better agreement with reference CP fluxes. We hypothesize that the use of 3 environmental variables makes the MLR approach more sensitive to site-specific factors, leading to larger residuals at sites where the tower complexity and/or sensor layout differs from that in Burba et al. (2008). Researchers should therefore document the specific correction type being used when applying the BC to OP NEE data. The BCs are a significant source of uncertainty, with impacts on flux estimates that were previously poorly characterized. Here, we demonstrate that the surface temperature model uncertainty alone is ~2 times the random flux error for the reference CP measurements.

Further, the performance of the corrections proposed in Burba et al. (2008) does not improve when site-specific temperature and heat flux measurements are used in place of the published semi-empirical models.

We find that the Wang approach benefits from direct calculation of the scaling parameters (*a* and *b*), which can only be performed during non-photosynthesizing periods. However, we also find that OP bias persists (Fig. 1 and 5) during photosynthetically active periods when direct calculation of *a* and *b* is not viable. Furthermore, the linearization of ΔNEE on *H* inherently assumes that the F_{OP} bias is positive at negative *H* and negligible at $H \approx 0$ Wm^{-2}, two assumptions that are contradicted by the data presented here (e.g. Fig. 2a) and in Järvi et al. (2009), thus casting doubt on the universal applicability of the Wang approach.

We recommend against applying the Fitting correction with coefficients optimized for other sites. We find here that the use of coefficients from Järvi et al. (2009) and Kittler et al. (2017) introduces larger uncertainties in F_{OP} than use of the BC SLR method. For most sites a side-by-side deployment of OP and CP flux measurements will not be feasible; in such cases the Fitting approach is not a viable solution for correcting either historic data or ongoing/future measurements.

We evaluated the suite of OP correction approaches that have been proposed in the literature and find that all of them reduce the bias in the derived long-term cumulative OP NEE; however, none appreciably improved the OP-CP correlation. Our results call into question core aspects of previous SPHE correction theories. In particular, our multiple linear regressions and neural network analyses revealed weak to negligible correlations between observed flux bias and parameters used in the above corrections. This raises the question of whether SPHE is in fact the primary physical cause of the observed OP biases and calls for the identification of additional bias sources.

An alternative hypothesis is that the CO_2 measurement biases arise from calibration drift. The OP measurements are more sensitive to such effects (e.g., arising from contaminated mirrors; Serrano-Ortiz et al., 2008), as both WPL terms are multiplied by the mean CO_2 concentration (Eq. 1). However, in this study the OP and CP analyzers were both calibrated simultaneously and on a regular basis using the same standards. Furthermore, a systematic concentration bias would amplify (or dampen) fluxes equally in both directions, and thus cannot explain the systematic OP CO_2 flux bias observed during the cold season. In fact, we find a large OP vs. CP NEE bias even immediately after calibrations when the corresponding 30-min average CO_2 concentrations were in

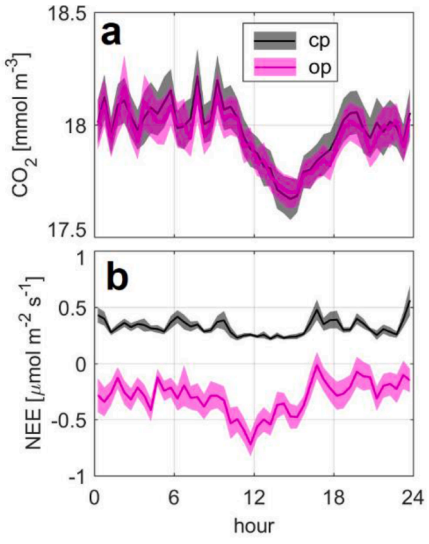

Fig. 7. Panel a shows the median diurnal CO_2 molar densities for the closed-path (black line) and open-path (magenta line) analyzers with standard errors (shaded areas) during December 2018. Panel b shows the corresponding median diurnal NEE values. Despite good agreement in the CO_2 concentration measurements (RMSE = 0.05 mmol m^{-3}), the NEE estimates imply fluxes that are opposite in sign, with enhanced biases around noon.

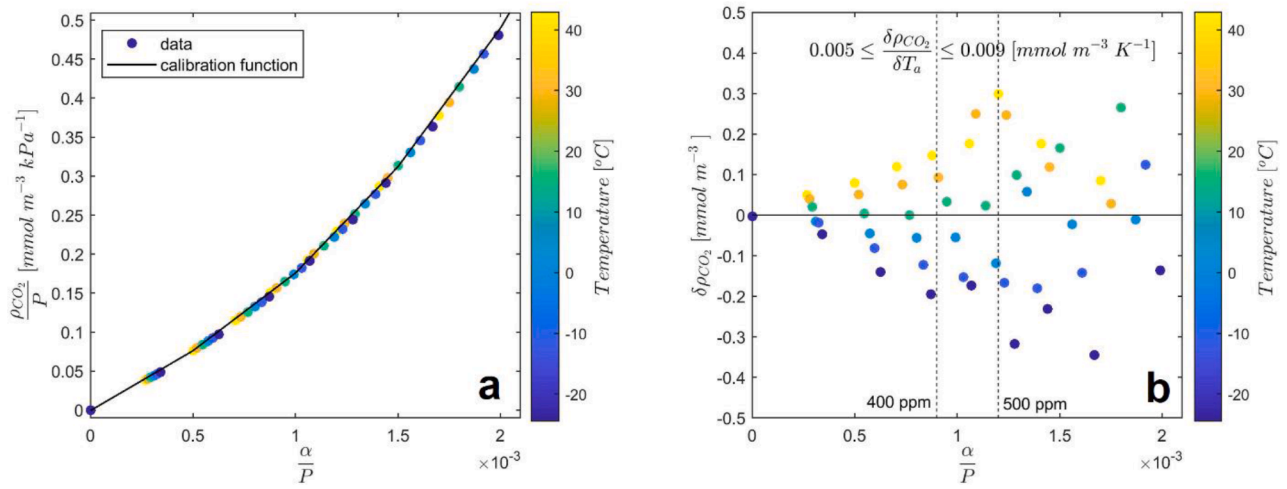

Fig. 8. Panel a shows the 5th-order polynomial calibration function (black line) relating measured CO_2 absorbance (α) to CO_2 molar density (ρ_{CO_2}) with both normalized by cell pressure (*P*). Datapoints are colored according to chamber temperature. Panel b shows the measured residuals from the calibration fit as a function of absorbance scaled by pressure and colored by temperature as in panel a. For visual guidance we overlaid the $\frac{\alpha}{P}$ range that is representative for ambient CO_2 levels (400 to 500 ppm) in dashed black lines.

excellent agreement (Fig. 7).

Another hypothesis is that the OP bias arises from inadequate spectroscopic corrections. For example, earlier studies have reported that the manufacturer-determined (water) broadening coefficients for the LI-7500 may be inadequate for accurate CO_2 concentration measurements (Edson et al., 2011; Kondo et al., 2014). Here we find larger OP biases with increasing ecosystem heat fluxes (section 3.3, Fig. 2a), a relationship that was invoked previously to identify spectroscopic errors for the IRGASON integrated OP analyzer (Campbell Scientific). The IRGASON couples sonic anemometry with IRGA measurements in a common sample volume and is thus unaffected by SPHE. Bogoev et al. (2015) and Helbig et al. (2016) reported that increasing the temporal resolution of temperature data used in the IRGASON spectroscopic calculations reduced OP biases by 1.6-3 fold. In our study we find a weaker ΔNEE : *H* relationship than reported by Helbig et al. (2016) ($R^2 = 0.12$ vs. $0.42 \leq R^2 \leq 0.91$) most likely because the LI-7500(A) is impacted by differing IRGA and sonic path heat fluxes whereas the IRGASON is not.

We investigated the temperature dependence of CO_2 absorption ($\frac{\delta\rho_{CO_2}}{\delta T_a}$) of the OP calibration that causes calibration errors proportional to the temperature changes of the air sample in the sensing path of the analyzer. As a result, when temperature fluctuations in the sensing path are correlated with vertical wind fluctuations, SPHE introduces a calibration-related bias in the CO_2 flux that is additive and proportional to the magnitude of the sensible heat flux in the sensor path. Here we find that the corresponding flux error is as large as 9 μmol m^{-2} s^{-1} per 1 K m s^{-1} kinematic heat flux (section 3.11; Fig. 8). Note that the temperature sensitivity ($\frac{\delta\rho_{CO_2}}{\delta T_a}$) depends on the IRGA calibration and will thus vary for other LI-7500 units. For our measurements at Bog Lake Peatland, the median winter/summer kinematic heat fluxes measured by the sonic anemometer were −0.005/−0.006 K m s^{-1}at night and 0.003/0.09 K m s^{-1} during daytime. This translates to median winter/summer temperature sensitivity-related flux errors of 0.045/0.054 μmol m^{-2} s^{-1} at night and 0.003/0.81 μmol m^{-2} s^{-1} during daytime. During winter, these errors are much smaller than the observed ΔNEE (Fig. 1a, median = −0.46 μmol m^{-2} s^{-1}). During summer, however, the computed errors offset the observed ΔNEE by 50%. Our direct wintertime measurements of SPHE show a systematic SPHE enhancement (due to sensor self-heating) of 0.01 K m s^{-1} (median). Thus, a more appropriate estimation of the $\frac{\delta\rho_{CO_2}}{\delta T_a}$ related measurement error in winter yields flux errors on the order of 0.1 μmol m^{-2} s^{-1}, or ~20% of observed ΔNEE.

As discussed in Section 3.4 and 3.5, the OP IRGA is subject to enhanced heat fluxes relative to those observed in the sonic measurement path. As a result, predictions of flux errors due to temperature sensitivities that rely on sonic measurements will be biased low. Sonic temperature measurements are hence not suitable for such corrections of the LI-7500 analyzer. Addressing this issue calls for spatially representative temperature measurements in the IRGA cell that are synchronized to the CO_2 absorption measurements. Such measurements would also enable direct quantification of SPHE without requiring the use of poorly-representative empirical parameterizations and thus could inform corrections for two OP measurement biases.

Overall, our observations of persistent temperature and heat gradients between the LI-7500(A) measurement path and the surrounding ambient air point to instrument path heat exchange (SPHE). Previously proposed SPHE correction theory is insufficient in reconciling observed differences between OP and CP fluxes. We also find evidence for temperature induced bias in CO_2 measurements when using the LI-7500 IRGA. As a result, the theoretical framework underlying current SPHE corrections (which neglects temperature sensitivity of the calibration residuals) is unable to reduce OP biases to within the uncertainty of closed-path flux measurements. This limits our ability to reliably characterize ecosystem carbon- and radiative forcing budgets using OP IRGAS. We show that the temperature sensitivity of the LI-7500 CO_2 absorbance measurements explains up to 50% of the observed growing season flux biases. Present SPHE correction approaches are not universally applicable as they do not explicitly account for calibration residual effects.

5. Conclusions & Recommendations

1. Open-path measurement bias prevails year-round during both day and night. It is therefore critical that appropriate corrections be applied over the entire measurement period.
2. Open-path sensor path heat exchange (SPHE) of the LI-7500 IRGA is internally and externally driven even at times when ambient temperatures exceed internal sensor temperatures.
3. Previously published correction methods are not universally applicable.
4. Dilution based SPHE corrections are insufficient to account for OP bias during the growing season when ecosystem heat fluxes are large.
5. There is evidence of additional OP measurement bias due to temperature dependences of the IRGA calibration. These are unaccounted for in SPHE theory.

6. Improper treatment of OP flux biases can change the magnitude and the sign of ecosystem carbon and radiative forcing budget calculations.
7. Use of current SPHE corrections (in the absence of a concurrent reference flux measurement) yields uncertainties that are larger than random flux errors—substantially degrading confidence in ecosystem carbon- and radiative forcing budgets.
8. Application of correction algorithms optimized for other sites introduces larger OP flux uncertainties than does the nominally universal SLR correction from Burba et al. (2008), and is thus not advised.
9. We call for a new OP correction framework that simultaneously characterizes SPHE and temperature induced measurement errors, which is only feasible with fast temperature measurements that are representative of the IRGA path.

Declaration of Competing Interest

The authors declare that they have no known competing financial interests or personal relationships that could have appeared to influence the work reported in this paper.

Acknowledgements

This work was supported by NASA's Interdisciplinary Research in Earth Science program (IDS Grant # NNX17AK18G), and by the United States Department of Agriculture National Institute of Food and Agriculture (USDA NIFA Grant 2018-67019-27808).

References

AMERIFLUX 2019. Dataset: BASE Measurement Height [Available online at https://ameriflux.lbl.gov/data/measurement-height/].

Amiro, B., 2010. Estimating annual carbon dioxide eddy fluxes using open-path analysers for cold forest sites. Agric. For. Meteorol. 150, 1366–1372. https://doi.org/10.1016/j.agrformet.2010.06.007.

Anthoni, P.M., Unsworth, M.H., Law, B.E., Irvine, J., Baldocchi, D.D., Tuyl, S.V., Moore, D., 2002. Seasonal differences in carbon and water vapor exchange in young and old-growth ponderosa pine ecosystems. Agric. For. Meteorol. 111, 203–222. https://doi.org/10.1016/S0168-1923(02)00021-7.

Baldocchi, D., Ryu, Y., Keenan, T., 2016. Terrestrial Carbon Cycle Variability. F1000Res 5, 2371. https://doi.org/10.12688/f1000research.8962.1.

Bingham, GE, Gillespie, CH, McQuaid, JH, 1978. Development of a miniature, rapid response CO2 sensor. Lawrence Livermore National Lab. Report UCRL-52440.

Bogoev, I., Helbig, M., Sonnentag, O, 2015. On the importance of high-frequency air-temperature fluctuations for spectroscopic corrections of open-path carbon dioxide flux measurement. Geophys. Res. Abstracts 17. EGU2015-2333. [Available online at. http://meetingorganizer.copernicus.org/EGU2015/EGU2015-2333.pdf.].

Broecker, W.S., Ledwell, J.R., Takahashi, T., Weiss, R., Merlivat, L., Memery, L., Peng, T.-H., Jahne, B., Munnich, K.O., 1986. Isotopic versus micrometeorologic ocean CO2 fluxes: A serious conflict. J. Geophys. Res. Oceans 91, 10517–10527. https://doi.org/10.1029/JC091iC09p10517.

Burba, G., Anderson, T., Komissarov, A., 2019. Accounting for spectroscopic effects in laser-based open-path eddy covariance flux measurements. Glob. Chang. Biol. 25, 2189–2202. https://doi.org/10.1111/gcb.14614.

Burba, G.G., McDermitt, D.K., Grelle, A., Anderson, D.J., Xu, L., 2008. Addressing the influence of instrument surface heat exchange on the measurements of CO2 flux from open-path gas analyzers. Glob. Chang. Biol. 14, 1854–1876. https://doi.org/10.1111/j.1365-2486.2008.01606.x.

Butterworth, B.J., Else, B.G.T., 2018. Dried, closed-path eddy covariance method for measuring carbon dioxide flux over sea ice. Atmos. Meas. Tech. 11, 6075–6090. https://doi.org/10.5194/amt-11-6075-2018.

Deventer, M.J., Griffis, T.J., Roman, D.T., Kolka, R.K., Wood, J.D., Erickson, M., Baker, J. M., Millet, D.B., 2019. Error characterization of methane fluxes and budgets derived from a long-term comparison of open- and closed-path eddy covariance systems. Agric. For. Meteorol. 278, 107638. https://doi.org/10.1016/j.agrformet.2019.107638.

Edson, J.B., Fairall, C.W., Bariteau, L., Zappa, C.J., Cifuentes-Lorenzen, A., McGillis, W. R., Pezoa, S., Hare, J.E., Helmig, D., 2011. Direct covariance measurement of CO2 gas transfer velocity during the 2008 Southern Ocean Gas Exchange Experiment: Wind speed dependency. J. Geophys. Res. Oceans 116. https://doi.org/10.1029/2011JC007022.

Finkelstein, P.L., Sims, P.F., 2001. Sampling error in eddy correlation flux measurements. J. Geophys. Res. Atmos. 106, 3503–3509. https://doi.org/10.1029/2000JD900731.

Fratini, G., Ibrom, A., Arriga, N., Burba, G., Papale, D., 2012. Relative humidity effects on water vapour fluxes measured with closed-path eddy-covariance systems with short sampling lines. Agric. For. Meteorol. 165, 53–63. https://doi.org/10.1016/j.agrformet.2012.05.018.

Fratini, G., McDermitt, D.K., Papale, D., 2014. Eddy-covariance flux errors due to biases in gas concentration measurements: origins, quantification and correction. Biogeosciences 11, 1037–1051. https://doi.org/10.5194/bg-11-1037-2014.

Gordon, I.E., Rothman, L.S., Hill, C., Kochanov, R.V., Tan, Y., Bernath, P.F., Birk, M., Boudon, V., Campargue, A., Chance, K.V., Drouin, B.J., Flaud, J.-M., Gamache, R.R., Hodges, J.T., Jacquemart, D., Perevalov, V.I., Perrin, A., Shine, K.P., Smith, M.-A.H., Tennyson, J., Toon, G.C., Tran, H., Tyuterev, V.G., Barbe, A., Császár, A.G., Devi, V. M., Furtenbacher, T., Harrison, J.J., Hartmann, J.-M., Jolly, A., Johnson, T.J., Karman, T., Kleiner, I., Kyuberis, A.A., Loos, J., Lyulin, O.M., Massie, S.T., Mikhailenko, S.N., Moazzen-Ahmadi, N., Müller, H.S.P., Naumenko, O.V., Nikitin, A. V., Polyansky, O.L., Rey, M., Rotger, M., Sharpe, S.W., Sung, K., Starikova, E., Tashkun, S.A., Auwera, J.V., Wagner, G., Wilzewski, J., Wcisło, P., Yu, S., Zak, E.J., 2017. The HITRAN2016 molecular spectroscopic database. Journal of Quantitative Spectroscopy and Radiative Transfer, HITRAN2016 Special Issue 203, 3–69. https://doi.org/10.1016/j.jqsrt.2017.06.038.

Grelle, A., Burba, G., 2007. Fine-wire thermometer to correct CO2 fluxes by open-path analyzers for artificial density fluctuations. Agric. For. Meteorol. 147, 48–57. https://doi.org/10.1016/j.agrformet.2007.06.007.

Grelle, A., Lindroth, A., 1996. Eddy-correlation system for long-term monitoring of fluxes of heat, water vapour and CO2. Glob. Chang. Biol. 2, 297–307. https://doi.org/10.1111/j.1365-2486.1996.tb00081.x.

Hanson J., P., Gill L., A., Xu, X., Phillips R., J., Weston J., D., Kolka K., R., Riggs S., J., Hook A., L., 2016. Intermediate-scale community-level flux of CO_2 and CH_4 in a Minnesota peatland: putting the SPRUCE project in a global context. Biogeochemistry 129, 255–272. https://doi.org/10.1007/s10533-016-0230-8.

Haslwanter, A., Hammerle, A., Wohlfahrt, G., 2009. Open-path vs. closed-path eddy covariance measurements of the net ecosystem carbon dioxide and water vapour exchange: A long-term perspective. Agric. For. Meteorol 149, 291–302. https://doi.org/10.1016/j.agrformet.2008.08.011.

Heikinheimo, M.J., Thurtell, G.W., Kidd, G.E., 1989. An open path, fast response IR spectrometer for simultaneous detection of CO2 and water vapor fluctuations. J. Atmos. Ocean. Technol. 6, 624–636. https://doi.org/10.1175/1520-0426(1989)006<0624:AOPFRI>2.0.CO;2.

Helbig, M., Wischnewski, K., Gosselin, G.H., Biraud, S.C., Bogoev, I., Chan, W.S., Euskirchen, E.S., Glenn, A.J., Marsh, P.M., Quinton, W.L., Sonnentag, O., 2016. Addressing a systematic bias in carbon dioxide flux measurements with the EC150 and the IRGASON open-path gas analyzers. Agric. For. Meteorol. 228–229, 349–359. https://doi.org/10.1016/j.agrformet.2016.07.018.

Hirata, R., Hirano, T., Mogami, J., Fujinuma, Y., Inukai, K., Saigusa, N., Yamamoto, S., 2005. CO2 flux measured by an open-path system over a larch forest during the snow-covered season. Phyton 45, 347–351.

Holl, D., Wille, C., Sachs, T., Schreiber, P., Runkle, B.R.K., Beckebanze, L., Langer, M., Boike, J., Pfeiffer, E.-M., Fedorova, I., Bolshianov, D.Y., Grigoriev, M.N., Kutzbach, L., 2019. A long-term (2002 to 2017) record of closed-path and open-path eddy covariance CO2 net ecosystem exchange fluxes from the Siberian Arctic. Earth Syst. Sci. Data 11, 221–240. https://doi.org/10.5194/essd-11-221-2019.

Horst, T.W., Lenschow, D.H., 2009. Attenuation of Scalar Fluxes Measured with Spatially-displaced Sensors. Bound.-Layer Meteorol. 130, 275–300. https://doi.org/10.1007/s10546-008-9348-0.

Ibrom, A., Dellwik, E., Flyvbjerg, H., Jensen, N.O., Pilegaard, K., 2007. Strong low-pass filtering effects on water vapour flux measurements with closed-path eddy correlation systems. Agric. For. Meteorol. 147, 140–156. https://doi.org/10.1016/j.agrformet.2007.07.007.

Järvi, L., Mammarella, I., Eugster, W., Ibrom, A., Siivola, E., Dellwik, E., Keronen, P., Burba, G., Vesala, T., 2009. Comparison of net CO2 fluxes measured with open- and closed-path infrared gas analyzers in an urban complex environment 14, 16. Boreal Environ. Res. 14, 499–514.

Jones, E.P., Ward, T.V., Zwick, H.H., 1967. A fast response atmospheric CO2 sensor for eddy correlation flux measurements. Atmos. Environ. 12, 845–851. https://doi.org/10.1016/0004-6981(78)90022-7.

Kittler, F., Eugster, W., Foken, T., Heimann, M., Kolle, O., Göckede, M., 2017. High-quality eddy-covariance CO2 budgets under cold climate conditions. J. Geophys. Res. Biogeosciences 122, 2064–2084. https://doi.org/10.1002/2017JG003830.

Kondo, F., Ono, K., Mano, M., Miyata, A., Tsukamoto, O., 2014. Experimental evaluation of water vapour cross-sensitivity for accurate eddy covariance measurement of CO2 flux using open-path CO2/H2O gas analysers. Tellus B 66, 23803. https://doi.org/10.3402/tellusb.v66.23803.

Lafleur, P.M., Humphreys, E.R., 2008. Spring warming and carbon dioxide exchange over low Arctic tundra in central Canada [WWW Document]. Glob. Chang. Biol. https://doi.org/10.1111/j.1365-2486.2007.01529.x.

Lee, X., Massman, W.J., 2011. A Perspective on Thirty Years of the Webb, Pearman and Leuning Density Corrections. Bound.-Layer Meteorol 139, 37–59. https://doi.org/10.1007/s10546-010-9575-z.

LI-COR Biosciences Inc. (2015): LI-7200 RS Enclosed CO2/H2O Gas Analyzer – Instruction Manual. Updated on Wednesday, November 13, 2019. Publication Number 984-15810, 226 pages.

Liu, H., Randerson, J.T., Lindfors, J., Massman, W.J., Foken, T., 2006. Consequences of Incomplete Surface Energy Balance Closure for CO2 Fluxes from Open-Path CO2/H2O Infrared Gas Analysers. Bound.-Layer Meteorol. 120, 65–85. https://doi.org/10.1007/s10546-005-9047-z.

Ma, J., Liu, R., Tang, L.-S., Lan, Z.-D., Li, Y., 2014. A downward CO 2 flux seems to have nowhere to go. Biogeosciences 11, 6251–6262. https://doi.org/10.5194/bg-11-6251-2014.

Massman, W.J., Lee, X., 2002. Eddy covariance flux corrections and uncertainties in long-term studies of carbon and energy exchanges. Agric. For. Meteorol., FLUXNET 2000 Synthesis 113, 121–144. https://doi.org/10.1016/S0168-1923(02)00105-3.

Moffat, A.M., Papale, D., Reichstein, M., Hollinger, D.Y., Richardson, A.D., Barr, A.G., Beckstein, C., Braswell, B.H., Churkina, G., Desai, A.R., Falge, E., Gove, J.H., Heimann, M., Hui, D., Jarvis, A.J., Kattge, J., Noormets, A., Stauch, V.J., 2007. Comprehensive comparison of gap-filling techniques for eddy covariance net carbon fluxes. Agric. For. Meteorol. 147, 209–232. https://doi.org/10.1016/j.agrformet.2007.08.011.

Moncrieff, J., Clement, R., Finnigan, J., Meyers, T., 2005. Averaging, Detrending, and Filtering of Eddy Covariance Time Series, in: Lee, X., Massman, W., Law, B. (Eds. Handbook of Micrometeorology: A Guide for Surface Flux Measurement and Analysis, Atmospheric and Oceanographic Sciences Library. Springer, Netherlands, Dordrecht, pp. 7–31. https://doi.org/10.1007/1-4020-2265-4_2.

Moncrieff, J.B., Massheder, J.M., de Bruin, H., Elbers, J., Friborg, T., Heusinkveld, B., Kabat, P., Scott, S., Soegaard, H., Verhoef, A., 1997. A system to measure surface fluxes of momentum, sensible heat, water vapour and carbon dioxide. J. Hydrol., HAPEX-Sahel 188–189, 589–611. https://doi.org/10.1016/S0022-1694(96)03194-0.

Nemitz, E., Mammarella, I., Ibrom, A., Aurela, M., Burba, G.G., Dengel, S., Gielen, B., Grelle, A., Heinesch, B., Herbst, M., Hörtnagl, L., Klemedtsson, L., Lindroth, A., Lohila, A., McDermitt, D.K., Meier, P., Merbold, L., Nelson, D., Nicolini, G., Nilsson, M.B., Peltola, O., Rinne, J., Zahniser, M., 2018. Standardisation of eddy-covariance flux measurements of methane and nitrous oxide. Int. Agrophys. 32, 517–549. https://doi.org/10.1515/intag-2017-0042.

Nobel, P.S., 1983. Biophysical Plant Physiology. W.H. Freeman and Company, San Francisco.

Olson, D.M., Griffis, T.J., Noormets, A., Kolka, R., Chen, J., 2013. Interannual, seasonal, and retrospective analysis of the methane and carbon dioxide budgets of a temperate peatland. J. Geophys. Res. Biogeosciences 118, 226–238. https://doi.org/10.1002/jgrg.20031.

Ono, K., Miyata, A., Yamada, T., 2008. Apparent downward CO2 flux observed with open-path eddy covariance over a non-vegetated surface. Theor. Appl. Climatol. 92, 195–208. https://doi.org/10.1007/s00704-007-0323-3.

Petrescu, A.M.R., Lohila, A., Tuovinen, J.-P., Baldocchi, D.D., Desai, A.R., Roulet, N.T., Vesala, T., Dolman, A.J., Oechel, W.C., Marcolla, B., Friborg, T., Rinne, J., Matthes, J.H., Merbold, L., Meijide, A., Kiely, G., Sottocornola, M., Sachs, T., Zona, D., Varlagin, A., Lai, D.Y.F., Veenendaal, E., Parmentier, F.-J.W., Skiba, U., Lund, M., Hensen, A., van Huissteden, J., Flanagan, L.B., Shurpali, N.J., Grünwald, T., Humphreys, E.R., Jackowicz-Korczyński, M., Aurela, M.A., Laurila, T., Grüning, C., Corradi, C.A.R., Schrier-Uijl, A.P., Christensen, T.R., Tamstorf, M.P., Mastepanov, M., Martikainen, P.J., Verma, S.B., Bernhofer, C., Cescatti, A., 2015. The uncertain climate footprint of wetlands under human pressure. PNAS 112, 4594–4599. https://doi.org/10.1073/pnas.1416267112.

Rebmann, C., Aubinet, M., Schmid, H., Arriga, N., Aurela, M., Burba, G., Clement, R., De Ligne, A., Fratini, G., Gielen, B., Grace, J., Graf, A., Gross, P., Haapanala, S., Herbst, M., Hörtnagl, L., Ibrom, A., Joly, L., Kljun, N., Kolle, O., Kowalski, A., Lindroth, A., Loustau, D., Mammarella, I., Mauder, M., Merbold, L., Metzger, S., Mölder, M., Montagnani, L., Papale, D., Pavelka, M., Peichl, M., Roland, M., Serrano-Ortiz, P., Siebicke, L., Steinbrecher, R., Tuovinen, J.-P., Vesala, T., Wohlfahrt, G., Franz, D., 2018. ICOS eddy covariance flux-station site setup: a review. International Agrophysics 32, 471–494. https://doi.org/10.1515/intag-2017-0044.

Reverter, B.R., Carrara, A., Fernández, A., Gimeno, C., Sanz, M.J., Serrano-Ortiz, P., Sánchez-Cañete, E.P., Were, A., Domingo, F., Resco, V., Burba, G.G., Kowalski, A.S., 2011. Adjustment of annual NEE and ET for the open-path IRGA self-heating correction: Magnitude and approximation over a range of climate. Agric. For. Meteorol. 151, 1856–1861. https://doi.org/10.1016/j.agrformet.2011.06.001.

Russell, E.S., Dziekan, V., Chi, J., Waldo, S., Pressley, S.N., O'Keeffe, P., Lamb, B.K., 2019. Adjustment of CO2 flux measurements due to the bias in the EC150 infrared gas analyzer. Agric. For. Meteorol. 276–277, 107593. https://doi.org/10.1016/j.agrformet.2019.05.024.

Sabbatini, S., Mammarella, I., Arriga, N., Fratini, G., Graf, A., Hörtnagl, L., Ibrom, A., Longdoz, B., Mauder, M., Merbold, L., Metzger, S., Montagnani, L., Pitacco, A., Rebmann, C., Sedlák, P., Šigut, L., Vitale, D., Papale, D., 2018. Eddy covariance raw data processing for CO2 and energy fluxes calculation at ICOS ecosystem stations. Int. Agrophys. 32, 495–515. https://doi.org/10.1515/intag-2017-0043.

Sebestyen, S.D., Dorrance, C., Olson, D.M., Verry, E.S., Kolka, R.K., Elling, A.E., Kyllander, R., 2011. Long-term monitoring sites and trends at the Marcell Experimental Forest. In: Kolka, R.K., Sebestyen, S.D., Verry, E.S., Brooks, K.N. (Eds.), Peatland Biogeochemistry and Watershed Hydrology at the Marcell Experimental Forest. CRC Press, NewYork, pp. 15–71, 2011.

Serrano-Ortiz, P., Kowalski, A.S., Domingo, F., Ruiz, B., Alados-Arboledas, L., 2008. Consequences of Uncertainties in CO2 Density for Estimating Net Ecosystem CO2 Exchange by Open-path Eddy Covariance. Bound.-Layer Meteorol. 126, 209–218. https://doi.org/10.1007/s10546-007-9234-1.

Shurpali, N.J., Verma, S.B., Clement, R.J., Billesbach, D.P., 1993. Seasonal distribution of methane flux in a Minnesota peatland measured by eddy correlation. J. Geophys. Res. Atmos. 98, 20649–20655. https://doi.org/10.1029/93JD02181.

Shurpali, N.J., Verma, S.B., Kim, J., Arkebauer, T.J., 1995. Carbon dioxide exchange in a peatland ecosystem. J. Geophys. Res. 100, 14319. https://doi.org/10.1029/95JD01227.

Wang, L., Lee, X., Wang, W., Wang, X., Wei, Z., Fu, C., Gao, Y., Lu, L., Song, W., Su, P., Lin, G., 2017. A Meta-Analysis of Open-Path Eddy Covariance Observations of Apparent CO2 Flux in Cold Conditions in FLUXNET. J. Atmos. Oceanic Technol. 34, 2475–2487. https://doi.org/10.1175/JTECH-D-17-0085.1.

Wang, W., Xu, J., Gao, Y., Bogoev, I., Cui, J., Deng, L., Hu, C., Liu, C., Liu, S., Shen, J., Sun, X., Xiao, W., Yuan, G., Lee, X., 2016. Performance Evaluation of an Integrated Open-Path Eddy Covariance System in a Cold Desert Environment. J. Atmos. Oceanic Technol. 33, 2385–2399. https://doi.org/10.1175/JTECH-D-15-0149.1.

Webb, E.K., Pearman, G.I., Leuning, R., 1980. Correction of flux measurements for density effects due to heat and water vapour transfer. QJR Meteorol. Soc. 106, 85–100. https://doi.org/10.1002/qj.49710644707.

Welles, J.M., McDermitt, D.K., 2005. Measuring Carbon Dioxide in the Atmosphere. In: Hatfield, J., Baker, J. (Eds.), Micrometeorology in Agricultural Systems. ASA-CSSA-SSSA, Madison, Wisconsin, pp. 287–320. https://doi.org/10.2134/agronmonogr47.c13.

Welp, L.R., Randerson, J.T., Liu, H.P., 2007. The sensitivity of carbon fluxes to spring warming and summer drought depends on plant functional type in boreal forest ecosystems. Agric. For. Meteorol. 147, 172–185. https://doi.org/10.1016/j.agrformet.2007.07.010.

Wohlfahrt, G., Fenstermaker, L.F., Iii, J.a.A., 2008. Large annual net ecosystem CO2 uptake of a Mojave Desert ecosystem. Glob. Chang. Biol. 14, 1475–1487. https://doi.org/10.1111/j.1365-2486.2008.01593.x.